Journal of Membrane Science 713 (2025) 123248

Contents lists available at ScienceDirect

Journal of Membrane Science

journal homepage: www.elsevier.com/locate/memsci

Nanofiltration membranes in asymmetric flow field-flow fractionation for improved organic matter size fractionation

Akhil Gopalakrishnan, Susan Treasa, Youssef-Amine Boussouga, Andrea I. Schäfer *

Institute for Advanced Membrane Technology (IAMT), Karlsruhe Institute of Technology (KIT), Hermann-von-Helmholtz-Platz 1, 76344 Eggenstein-Leopoldshafen, Germany

ARTICLE INFO

Keywords:
Natural organic matter (NOM)
Dissolved organic matter (DOM)
Membrane fouling
Molecular weight cut-off (MWCO)
Size separation

ABSTRACT

Size fractionation of organic matter (OM) by asymmetric flow field-flow fractionation (FFFF) with ultrafiltration (UF) is limited by solute loss and peak resolution, particularly for low molecular weight fractions (<10 kDa). Nanofiltration (NF) with a molecular weight cut-off (MWCO) of ≤1 kDa can achieve significant OM retention and may improve OM fractionation. NF membranes with MWCOs ranging from 0.3 to 3 kDa were used to evaluate the retention and fractionation of nine OMs in the humic, polyphenol, biopolymer, and low molecular weight organic classes in stirred cell NF and FFFF. Membranes with an MWCO of 0.2–0.3 kDa (with a pure water permeability of 5–16 $L.m^{-2}.h^{-1}.bar^{-1}$) with low OM interaction exhibited high peak recovery and resolution and hence improved OM fractionation. Loose NF (MWCO 3 kDa) exhibited a poor peak recovery because of a high OM loss due to both adhesion and permeation, particularly at high ionic strengths (>10 mM). A mixture of nine types of OM and natural organic matter samples from rivers, swamps and lakes achieved good fractionation with a 0.3 kDa (NF270) membrane at low ionic strength. The performance of NF for the analysis of OM and colloids in the smallest size range (≤1 kDa MW) could be further improved by optimizing the salt composition of the mobile phase and by overcoming the pressure limitations of FFFF channels.

1. Introduction

Natural organic matter is a ubiquitous, complex mixture of naturally occurring macromolecular humic and non-humic components [1–4], which vary widely in molecular size and structures, leading to diverse properties [5,6]. The composition of organic matter (OM) in water varies with its source, the water chemistry, temperature, pH, biological processes, location, and seasons [5]. OM impacts aquatic life by altering oxygen levels, attenuating UV-B radiation, and influencing the solubility, toxicity, bioavailability, mobility, and distribution of trace elements and micropollutants [7–9].

The wide range of molecular weight distribution (polydispersity), complex structure, and multiple functional groups of natural organic matter (NOM) influence the binding and transport of contaminants [10–12]. There is ample evidence in the literature to suggest that OM composition during treatment and throughout the distribution system influences water quality and overall potential health risks [13]. In water treatment, low molecular weight OM size fractions (i.e., <1 kDa) may contribute to bacterial regrowth [14,15] and have significantly higher specific disinfection by-product formation potential [16–18] and chemically irreversible fouling potential [19]. On the other hand, high molecular weight (≥100 kDa) [20] and hydrophilic [21,22] fractions have more reversible fouling potential, and hydrophobic and high molecular weight OM fractions generate chlorination by-products [23]. It is crucial to understand OM composition to optimize water treatment protocols. However, OM characterization is challenging and typically yields method-specific results that are cumbersome to link with the mechanisms and dynamics of OM [24,25].

OM fractionation and size distribution analysis help to characterize complex OM components with specific sizes and physicochemical properties. Size fractionation (separation to constituents/fractions) is relevant for OM reactivity assessment during drinking water disinfection [16,26] and for predicting membrane fouling [27–31]. Size distribution analysis helps to understand complex interactions in treatment processes, develop more efficient treatment protocols, and determine the membrane molecular weight cut-off (MWCO) for contaminants [32]. Common OM fractionation techniques rely on chemical properties (hydrophobicity and polarity) and physical properties (hydrodynamic size). Techniques such as resin fractionation, polarity rapid assessment, and reversed-phase high-performance liquid chromatography rely on OM

* Corresponding author.
E-mail address: Andrea.Iris.Schaefer@kit.edu (A.I. Schäfer).

https://doi.org/10.1016/j.memsci.2024.123248
Received 28 June 2024; Received in revised form 5 August 2024; Accepted 25 August 2024
Available online 26 August 2024

hydrophobicity and polarity [26]. Field-flow fractionation, ultrafiltration (UF), high-performance size exclusion chromatography, gel permeation chromatography, ultracentrifugation, dialysis, laser desorption Fourier transform mass spectrometry, and vapor pressure osmometry are based on OM size distribution and stationary phase affinity [26,32].

Each OM fractionation technique has individual drawbacks, method-specific results, and challenges when fractionating large and small OM fractions. The most common size fractionation technique, high-performance size exclusion chromatography, separates OM fractions by their inclusion or exclusion from a resin-packed column's pores. Large OM (molar mass $> 10^6$ kDa) size exclusion chromatography is limited by column-OM interactions and shear degradation (inability to resist mechanical stress) induced by the flow through a packed column [33–35]. Low molecular weight OM analysis is challenging [36] in high-performance size exclusion chromatography and gel permeation chromatography due to sample loss by adsorption in the stationary phase [37,38] and in ultrafiltration (UF), nanofiltration (NF), and flow field-flow fractionation due to OM loss caused by membrane-OM interactions [19,39] and permeation due to OM smaller than the membrane's MWCO. Other challenges include poor resolution [40] and incompatibility of available detectors with small size ranges [41]. Thus, the development of an analytical technique for non-perturbing and accurate size characterization of a wide size range of OM is desirable [36].

Asymmetrical Flow Field-Flow Fractionation (FFFF) is a separation technique used to analyze nanoparticles, macromolecules, and colloidal particles based on their size [42,43]. FFFF uses the flow of a mobile phase over a membrane to separate an OM mixture (polydisperse sample) in a wide size range of 1 nm–100 μm [34,44,42]. When an OM mixture is injected into the FFFF channel, particles of different sizes are separated based on their diffusion coefficients. The driving force (permeate drag force, F_{Dp}) exerted on particles depends principally on the applied permeate flow velocity, u_p (m.s^{-1}), mobile phase viscosity, η (kg.m^{-1}.s^{-1}), and equivalent volume hydrodynamic diameter, d_e (m), as expressed using the Stokes' law [45–47] in Eq. (1).

$$F_{Dp} = 3 \cdot \pi \cdot \eta \cdot d_e \cdot u_p \tag{1}$$

According to the FFFF theory [34,48], OM types with the same diffusion coefficient form equilibrium layers due to a balance between the diffusion of the solute and the permeate drag created by the flow of the mobile phase. The thickness of the equilibrium layer, l, depends on the permeate flow-induced velocity and the particles' diffusion coefficient. The fundamental relationship that associates FFFF parameters such as the applied permeate flow velocity, Q_p (m^3.s^{-1}), the channel height, h (m), and the void volume (effective separation volume of the channel), V_0 (mL), with the OM property such as the diffusion coefficient, D (m^2.s^{-1}), is the retention parameter, λ (dimensionless) [42,48,43], given in Eq. (2).

$$\lambda = \frac{V_0 \cdot D}{Q_p \cdot h^2} \tag{2}$$

The retention parameter, λ can be considered a fundamental parameter that links the FFFF theory with the observed entities. The separation of peaks during fractionation in FFFF can be predicted as a function of the retention parameter utilizing the peak retention ratio (commonly referred to as "retention ratio" in the literature) [42,48,49], as given in Eq. (3).

$$\textit{Peak retention ratio} = 6\lambda\left(\coth\frac{1}{2\lambda} - 2\lambda\right) \tag{3}$$

Under high sample retention conditions, λ approaches zero, and the peak retention ratio becomes 6λ [43]. The peak retention ratio can be experimentally determined as the ratio of the void time (the retention time of the first peak originating from unretained components) and the OM retention time (Fig. 1). In addition to the peak retention ratio, peak recovery and peak resolution can be used to evaluate the quality of the signal and the separation of the different components during the fractionation.

In FFFF, fractionation occurs through solute interactions with an external field without a stationary phase, providing a molar mass distribution with less shearing degradation than size exclusion chromatography [33,34] (see Table S1). FFFF can non-destructively separate particles of size 1 nm to 100 μm [34,44,42]. FFFF of OM, particularly small OM in the size range of 500–1000 Da (hydrodynamic size of approximately 1 nm), such as humic acid, is limited by sample losses (indicated by poor peak recovery) due to poor OM retention and OM

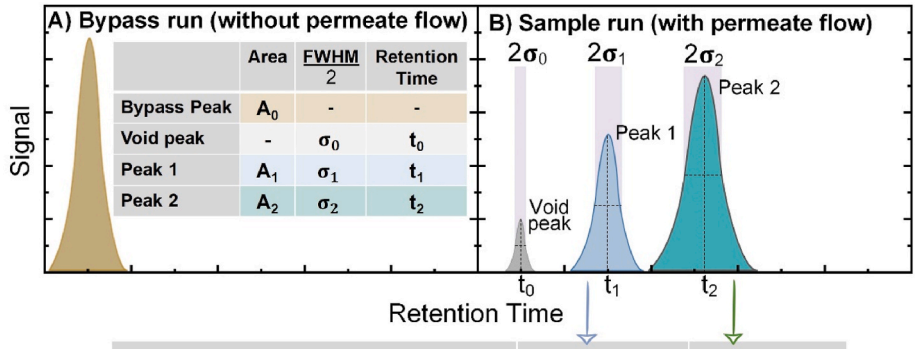

C) FFFF performance parameters	Peak 1	Peak 2
$\text{Peak Recovery} = \frac{A}{A_0}\cdot 100$	$\frac{A_1}{A_0}$	$\frac{A_2}{A_0}$
$\text{Peak Resolution} = \frac{\Delta t}{2(\sigma_1+\sigma_2)}$	$\frac{t_1 - t_0}{2(\sigma_0+\sigma_1)}$	$\frac{t_2 - t_0}{2(\sigma_0+\sigma_2)}$
$\text{Peak Retention Ratio} = \frac{t_0}{t_R}$	$\frac{t_0}{t_1}$	$\frac{t_0}{t_2}$

Fig. 1. Schematic representation of A) sample eluted through a capillary bypassing the FFFF channel without permeate flow for maximum recovery of sample, B) sample eluted over the membrane in the channel with permeate flow, C) estimation of fractionation parameters based on the area, retention time, and the full width at half maximum (FWHM) of peaks.

deposition on membranes [50,51]. A further limitation is poor peak resolution due to peak overlapping and broadening, reducing the accuracy and precision of molecular weight determination of the OM, especially for low molecular weight fractions [36,39,40].

The lower size limit of fractionation in FFFF is set by the membrane's MWCO [35,36,42]. Although lower MWCO membranes retain smaller OM species, their use in FFFF is limited by their low permeability [36,52]. A tight NF membrane limits the permeate flow rate, reducing the permeate drag force (see Eq. (1)) required for solute separation. NF membranes can potentially increase the peak recovery of low molecular weight fractions without losing the peak resolution if a sufficient permeate flow (typically 2.0–3.0 mL.min^{-1} corresponding to a flux of approximately 36–54 L.m^{-2}.h^{-1}) can be maintained. However, NF membranes are unsuitable for some commercially available FFFF configurations due to low membrane permeability, which demands a high transmembrane pressure. Consequently, FFFF typically uses UF membranes, which allow for higher permeate flow rates, providing the necessary drag force for effective solute separation. Additionally, a historical preference for UF membranes during the early periods of development and applications of FFFF established a standard practice and technological familiarity within the field [43,53]. There is an emerging interest in NF membranes for FFFF applications to improve the fractionation of OM in natural waters [52,54] and the characterization of metal-OM associations in natural [52,55–59] and synthetic waters [60,61]. Typical NF membranes have a MWCO for dissolved organic solutes between 0.2 and 1.0 kDa and a 20–80% sodium chloride rejection [62]. The MWCO transition from NF to UF (from 0.5 to 10 kDa [63–66]) is not clearly defined in membrane literature [67]. Membranes with large MWCOs in the range of 0.5–2.0 kDa and high permeation of salts, including monovalent and multivalent salts, often termed loose NF membranes [68], may bridge the gap between UF membranes and tight NF membranes in FFFF.

UF membranes (MWCO $\geq$1 kDa or pore size $\geq$2 nm) are predominantly used for OM fractionation in FFFF [53,69–76]. The most widely used membrane MWCO for FFFF ranges from 5 to 30 kDa [34,47,77–79]. MWCO 0.3–20.0 kDa membranes (summarized in Table S2 [51,55,73,75,80–82]) have been used to analyze OM with FFFF. In membrane filtration, both UF and NF membranes are widely used for OM removal and fractionation [83–87]. Membrane nominal MWCO (in kDa) and membrane pore diameter (in nm) are frequently used to categorize size fractionation using membrane filtration [88,89], with MW and pore size correlated using the Worch equation [87,90]. MWCO, defined by 90% solute retention [91], isn't fully reliable for OM size fractionation due to variations in pore sizes or MWCO distribution, influenced by the shape and charge of probe solutes [67,83].

To improve the separation and resolution in FFFF, it is important to examine sample loss, particularly the deposition of OM on the membranes.

Sample loss due to membrane-OM interaction: OM-membrane interactions are principally adhesive [92] and electrostatic [51,93]. The term adhesive interaction of OM is a broad term that represents the "stickiness" of an OM to membrane surface by the collective contributions of diverse specific interactions such as mechanical interlocking, van der Waals interaction, covalent bonding (bridging), hydrophobic interactions, and hydrogen bonding as described for various OM by Cai et al. [92]. Such interactions alter retention time and peak recovery, while peak resolution is reduced by peak distortion and broadening, making fractograms unrepresentative of the actual MW distribution [36,94,95]. Membrane characteristics, such as pore diameter/MWCO [47,77], charge, roughness [77,96], swelling, and surface functionalities [50,77,95] contribute to OM-membrane interactions in FFFF, influencing size distribution outcomes. Membranes with negative charge and lower affinity for OM exhibit low adhesion, but van der Waals interactions, hydrogen bonding, and hydrophobic interactions can enhance adhesion [92].

Sample loss due to low OM retention: OM retention and fractionation is influenced by OM's chemical (e.g., hydrophobicity, charge) and physical (e.g., size, shape) properties, as well as the solution's properties (e.g., pH, ionic strength, presence of complexing cations) [85,97,98]. Peak recovery of a fraction represents the amount of that fraction retained by the membrane (see Fig. 1). The reduction in OM retention with the nominal membrane MWCO [54] reduces peak recovery and signal strength, especially for fractions smaller than the membrane pore size [47,99]. Due to deviations between apparent MWCO and the manufacturer's nominal MWCO [54] and wide membrane pore size distribution, the actual sample loss across the membrane can be higher than expected. A tighter membrane with higher OM matter retention may minimize OM loss.

Low resolution due to low flux and poor drag force: In principle, FFFF can fractionate samples of any size, while resolution is determined by the difference in drag force. Using a tighter (low MWCO) membrane to retain small fractions may counteract the requirement for high permeate flow rates to generate the permeate drag force required for effective fractionation. Using a low permeate flow rate ($\leq$2.0 mL.min^{-1}) could adversely affect low molecular weight fractionation since the equilibrium between solute mass transfer towards the membrane (due to the permeate drag-induced field) and away from the membrane (due to diffusion driven by a subsequent concentration gradient) is disturbed [35].

Given the discussed limitations and challenges, five NF membranes with different MWCOs and material types were used to evaluate the FFFF fractionation of nine types of OM from the humic, polyphenol, biopolymer, and low molecular weight organic classes. The resulting peak recovery was further elucidated by evaluating OM retention using NF in stirred cell experiments. To demonstrate the applicability of the method for characterizing NOM, surface water samples collected from various lakes, swamps and rivers across four different countries were fractionated. The specific research questions addressed are.

i) How do different NF membranes affect the fractionation (peak recovery and peak resolution) of OM in FFFF?
ii) How do OM peak recovery and peak resolution of OM change with the ionic strength for NF/UF membranes in FFFF?
iii) Do electrostatic, adhesive, and permeate drag interactions between OM and NF membranes alter fractionation at varying ionic strengths in FFFF?

Membranes are frequently used in both FFFF and membrane filtration for OM fractionation, yet the literature, terminology, and underlying concepts in these fields are often misaligned. Efforts are made to bridge this gap, aiming to provide insights accessible to both the analytical FFFF and membrane filtration communities.

2. Materials and methods

2.1. Asymmetric flow field-flow fractionation system

An AF2000 Multiflow asymmetric flow field-flow fractionation (FFFF) system (Postnova Analytics GmbH, Landsberg, Germany) was coupled with a UV–Vis detector (PN3212, Postnova, Germany) and an organic carbon detector (OCD, Model 9, DOC-Labor, Germany) in series using capillary tubes (1/16-inch outer diameter, 0.007-inch inner diameter, 1.5 m length between UV-Vis and OCD). The membrane channel was created by sandwiching NF membrane coupons (29.5 cm $\times$ 3.0 cm) between a porous ceramic frit at the bottom and a polyester-based spacer of thickness 500 μm (specification provided by the manufacturer) at the top. The spacer pressed on the top of the membrane created a trapezoidal channel with an active membrane area of 33.4 cm^2. A detailed description of the system has been published elsewhere [47,60,92].

The FFFF protocol is provided in Tables S6 and S7. FFFF channel has a feed flow (commonly referred to as injection/tip flow in FFFF

literature) that carries the OM sample and mobile phase, a focus flow of the mobile phase applied opposing to the feed flow to offer a relaxation period before the longitudinal transport of samples, a concentrate flow (commonly referred to as channel out flow or detector flow), and a permeate flow (commonly referred to as 'crossflow' in FFFF literature) across membrane surface as illustrated in Fig. 2 and Fig. S1. Briefly, a permeate flow rate (Q_p) of 3.0 mL.min^{-1}, concentrate flow rate (Q_c) of 0.5 mL.min^{-1}, and focus flow rate (Q_{foc}) of 3.4 mL.min^{-1} were used based on the method adapted from Cai et al. [92]. The focus time was 4 min, and the total run time, including equilibrium delay time and rinsing, was 130 min. A higher pressure is required with tight NF membranes to achieve a sufficiently high (≥2.0 mL.min^{-1}) permeate flow rate. FFFF channel pressure limit on the permeate syringe pump is typically 15 bar [100]; a high flow rate set with tight NF membranes results in a pressure drop and bubble buildup on the permeate side due to a low mobile phase volume passing through the membrane. Using thin capillary tubing (e.g., 0.1 mm inner diameter) could provide back pressure in the channel to maintain a sufficient volume of mobile phase within the channel under high permeate flow rates [101]. For membranes with a MWCO of 1 kDa or less, a 50 cm back pressure tubing was used, whereas for membranes with a MWCO of 3 kDa, a 40 cm back pressure tubing was used. Any potential variations in hydrodynamic forces during fractionation, due to differences in back pressure tubing length, were deemed negligible. The permeate pressure limit was manually increased from 15 to 18 bar in the system configuration to prevent the FFFF system from automatically shutting down due to permeate overpressure.

For the mobile phase for FFFF, 1 mM phosphate buffer of pH 6.9 ± 0.2 was prepared by mixing 0.45 g KH_2PO_4 (EMSURE, Merck Millipore, Germany) and 0.27 g Na_2HPO_4 (EMSURE, Merck Millipore, Germany) in 5 L of MilliQ water (MilliQ A+ system, Millipore, Germany). For ionic strength experiments, 0–100 mM $NaNO_3$ (EMSURE, Merck Millipore, Germany) was added to 1 mM KH_2PO_4 and Na_2HPO_4 buffer at pH 6.8. $NaNO_3$ was selected to vary the ionic strength as it is one of the salts with minimal retention in NF. Using a salt with high retention in NF at a high concentration would lead to a salt concentration gradient at the membrane surface by concentration polarization. Peak retention ratio, peak recovery, and peak resolution, as well as the estimation of electrostatic forces, hydrodynamic forces, and mass loss due to adhesion, were calculated using methods reported elsewhere [47,92] (see Table 2).

2.2. Nanofiltration system

OM retention and permeability were evaluated in dead-end mode to characterize the NF membranes. Filtration was carried out in a stainless steel (SS) stirred cell having a volume of 900 mL and a filtration area of 38.5 cm^2 at constant flux conditions at 400 rpm and 20 ± 3 °C. A detailed system description has been published elsewhere [102,103]. The protocol is provided in Table S5. Membrane performance during OM transport in stirred cells (retention, solute flux, and solute permeability) was evaluated based on the equations listed in Table 2. Fig. 2 presents a schematic representation of the stirred cell and the FFFF channel. Fig. S1 gives a detailed schematic of the stirred cell filtration and FFFF systems.

2.3. Nanofiltration membranes

Commercial NF membranes were selected to cover a wide range of membrane surface characteristics and performance in the tighter membrane regime (Table 1). The highest permeate flow rates that can be used in FFFF depend on membrane permeability. Membranes with water permeability ≥5 L.m^{-2}.h^{-1}.bar^{-1} were found to be compatible with the permeate flow rate of 3.0 mL.min^{-1} used in FFFF. A permeate flow rate of 3.0 mL.min^{-1} with a membrane area of 33.4 cm^2 corresponds to a flux of approximately 54 L.m^{-2}.h^{-1}. The permeate flow rate was regulated at 0.2 mL.min^{-1} using a flow-regulating needle valve in the stirred cell with a membrane area of 38.5 cm^2 to maintain a permeate flux consistent with FFFF.

The 3 kDa MWCO membrane (HY10) used in this work is regarded as a loose NF membrane [61] following the general criteria of having a large MWCO with neutral species in the range of 500–2000 Da and high permeation of salts, including monovalent and multivalent salts [68]. A HY70 membrane with a very low water permeability of 2 L.m^{-2}.h^{-1}.bar^{-1} was not considered for the FFFF experiments as the permeate flow rate of 3.0 mL.min^{-1} used in the FFFF protocol (Table S1) could not be achieved under the channel pressure limit of 15 bar.

The zeta potential of the membranes was calculated from streaming potential measurements at pH 2.5–10. The protocol followed for the streaming potential determination is given in Table S8.

2.4. Organic matter types

The study used nine different types of OM: humic acid (HA) (Technical®, Sigma Aldrich, Germany), tannic acid (TA) (ACS, Alfa Aesar, USA), sodium alginate (SA) (Catalog no. B25266, low viscosity, 72–78% purity, Alfa Aesar, Germany), tannin (TAN) (L19125, PEP 65% purity, exGrape PEL, Grap'sud, France), tea leaf extract (Tea) (Tata Tea, batch No. 09PP45-1, packaged 05.2018, India), fermented product (FP) (Rechtsregulat® Bio, Dr. Niedermaier Pharma GmbH, Germany), Australian NOM (AUS), worm farm extract (WF) (Schäfer household, November 2019, Karlsruhe, Germany), and bovine serum albumin (BSA) (Sigma Aldrich, Germany). The detailed properties of the different types of OM are summarized in Table S3. 1 g.L^{-1} stock solutions of HA, TA, Tea, AUS, TAN, and SA were prepared in Milli-Q water. OM stock solutions (except for BSA) were filtered through 0.45 μm cellulose acetate filters (Millisart, Sartorius, Germany) to remove suspended particles and stored in a cool (5 °C) and dark place. To enhance the solubility of HA, 1 g of NaOH (pellet, purity ≥99.9%, Merck, Germany) was added to the HA stock solution and stirred for 24 h, resulting in a pH of 11–13. The pH of the stock solution was adjusted to 8 with HCl before use. BSA stock was prepared with slow stirring to avoid denaturation of the protein induced by mechanical shear [111]. FP was supplied as a viscous liquid

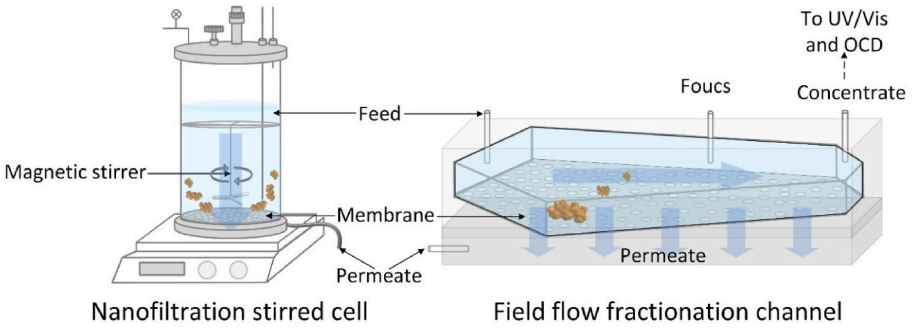

Fig. 2. Schematic of stirred cell and FFFF channel used for OM filtration and fractionation using NF membranes.

Table 1
Properties of the nanofiltration membranes used in FFFF and the stirred cell.

Membrane	Supplier	MWCO (Da)[a]	Active layer material[a]	Pure water permeability ($L.m^{-2}.h^{-1}.bar^{-1}$) [b]	NaCl retention (%)[a]	Zeta potential (mV)
NF90	DuPont, USA	90–180 [104]	Aromatic polyamide [105]	9 ± 2	85–90 [106]	−62 ± 4[e]
NF270	DuPont, USA	150–340 [104]	Semi-aromatic piperazine based polyamide [105]	16 ± 3	40–60 [106]	−55 ± 5[d] [60]
PES300[c]	Postnova, Germany	300 [107]	Polyethersulfone (PES) [107]	5 ± 1	23 ± 5[d]	−77 ± 5[e]
HY50	Hydranautics Nitto, USA	1000 [108]	Sulfonated Polyethersulfone [108]	6 ± 1	55 [108]	−33 ± 1[d] [61]
HY10	Hydranautics Nitto, USA	3000 [108]	Sulfonated Polyethersulfone [108]	54 ± 5	20 [108]	−38 ± 1[d] [61]

[a] Based on previous reports and product datasheets from the manufacturers.
[b] Data from this work, measured in stirred cell filtration.
[c] Supplier product code: AF2000 MF-AF4 Analytic PES Membrane, Z-AF4-MEM-611-300D [107].
[d] Measured with 5 and 10 mM NaCl.
[e] Data from this work, measured with 1 mM KCl at pH 6.9, corresponding to the molarity and pH of the FFFF mobile phase.

at approximately 50000 $mgC.L^{-1}$, which was diluted to make stock solutions. The extracted liquid from the worm farm was used as WF stock solution at a concentration of 400–600 $mgC.L^{-1}$. TA, TANN, Tea, and BSA solutions were used within two days of stock preparation since they have been observed to be susceptible to mold growth and hydrolysis. Feed solutions in filtration experiments contained 13 ± 3 $mgC.L^{-1}$ OM at pH 8.0 ± 0.2 with the background electrolytes 1 mM $NaHCO_3$ (Bernd Kraft, purity ≥99.7%, Germany) and 10 mM NaCl (VWR chemicals, purity ≥99.9%, Germany), diluted from the respective stock solutions in Milli-Q water.

Surface water samples were collected from three tropical countries in sub-Saharan Africa (Ghana, Tanzania, and The Gambia) [14,112,113], and the Black Forest (Germany) [114,115], where high concentrations of natural organic matter (NOM) had previously been reported. The water sources included four rivers, two lakes, a swamp, a swamp lake, and a wastewater. Table S4 summarizes the sampling details and the water quality of the samples used for fractionation in FFFF.

The fractionation of standard OM with known MWs in the FFFF-OCD with different membranes was performed using 15 ± 2 $mgC.L^{-1}$ poly (styrene sulfonate) sodium salt (PSS) (Polymer Standards Service GmbH, Mainz, Germany) of nominal MWs 1, 2, 10, 67, 140, and 280 kDa. PSS is considered an ideal molecular weight standard for validating the fractionation of NOM due to its comparable density, molecular conformation, charge density, and hydrodynamic properties [47,53,116]. The molar mass at the peak maximum (M_p) measured with GPC/SEC, as reported by the manufacturer, is 891, 2180, 9740, 65400, 151000, and 258000 Da, respectively. Table S3 summarizes the carboxylic and phenolic acidity and the net anionic charge of the OM.

2.5. Water analysis

The dissolved organic carbon (DOC) of the OM samples was measured for the stock, feed, permeate, and concentrate as non-purgeable organic carbon (NPOC) using a total organic carbon analyzer (TOC-L CPH, Shimadzu, Japan). Surface water samples were filtered with 0.45 μm cellulose acetate filters (Millisart, Sartorius, Germany) to remove suspended particles before analysis. Consequently, the analyzed samples represent the dissolved organic matter (DOM) in the respective surface waters. The samples were acidified with 1.5% of the sample volume of 1 M HCl (Bernd Kraft, Germany), then sparged with N_2 gas at a flow rate of 100 $mL.min^{-1}$ to strip off any purgeable organic and inorganic carbon. The sample was then injected into a combustion tube at 680 °C for catalytic oxidation and finally analyzed with non-dispersive infrared detection.

The OM fractions in the permeate samples of stirred cell NF experiments were analyzed using a liquid chromatography-organic carbon detector (LC-OCD)-organic nitrogen detector (OND) (Model 9, DOC Labor, Germany) and a UV-detector at 254 nm without being coupled to FFFF. An SEC column (Toyopearl 341 HW50–S, Tosoh Bioscience, Japan) was used to separate OM based on the size of the organic fractions and their secondary interactions with the hydroxylated methacrylic polymer resin in the column. A detailed description of the protocol is given by Huber et al. [117]. Potassium hydrogen phthalate (KHP) was used for OCD and TOC calibrations (see calibration graphs in Figs. S3 and S4).

The specific ultraviolet absorbance (SUVA) of feed and permeate was calculated as the ratio UV_{254}/DOC ($L.cm^{-1}.mg^{-1}$) (Fig. S16). It was determined by measuring the absorbance of samples at 254 nm by using UV/Vis (UV/Vis Spectrometer, Lambda 25, PerkinElmer, USA). The pH value of samples and feed solution was measured using a pH meter (pH/Cond 3320, WTW, Germany) with a pH sensor (SenTix® 41, WTW, Germany). The turbidity of surface water samples was analyzed using a turbidity meter (AL250T-IR, Aqualytic, Germany).

2.6. Data calculation

The equations used for various calculations are described in Table 2 and Table S9. Peak recovery (Eq. (4)) corresponds to the ratio of peak area obtained with and without a permeate flow. Peak recovery was calculated from peak areas that correspond to the peaks eluting during the initial 70 min of the Elution I phase (see Table S6) when there is a permeate flow. Aggregates or higher molecular weight fractions adhering to the membrane due to the permeate drag that could elute when the permeate flow is stopped in the Elution II phase are not included in the recovery calculation. Normalized peak recovery (Eq. (5)) indicates the relative peak recovery of different OM types for a given membrane. If a membrane achieves 100% normalized peak recovery of an OM, this indicates the highest observed peak recovery for that membrane. Conversely, 0% normalized peak recovery indicates the lowest observed peak recovery among all OM types for that membrane.

Peak resolution (Eq. (7)) gives a measure of the separation of two peaks of different retention times. The mass loss due to adhesive interaction was estimated as an indicator for the extent of adhesive interaction of OM with NF membrane by following the protocol described elsewhere [92]. Mass $loss_{adhesion}$(%) was calculated by subtracting the OM mass eluted over the membrane and OM mass permeated through the membrane, from the mass in the feed as given in Eq. (10). Therefore, mass loss due to the permeation through the membrane was excluded for the calculation of the mass loss due to adhesion.

The permeate drag force was estimated (Eq. (11)) based on the hydrodynamic diameter determined from FFFF retention time and the electrostatic force was estimated based on the surface potential of OM (Eq. (12)) [118,119] and NF membranes (assumed to be equal to membrane zeta potential, Table 1) [47].

Table 2
Calculation parameters and equations for FFF and NF performance evaluation [109,110].

FFFF parameters	Formula	Eq.
Peak recovery (%)	$Peak\ recovery = \frac{A}{A_0}\cdot 100$	(4)
Normalized peak recovery (%)	$Norm.peak\ recovery = \frac{(X - X_{min}) \bullet 100}{(X_{max} - X_{min})}$	(5)
Peak retention ratio (−)	$Peak\ retention\ ratio = \frac{t_0}{t_R}$	(6)
Peak resolution (−)	$Peak\ resolution = \frac{\Delta t}{2(\sigma_1 + \sigma_2)}$	(7)
NF parameters		
Retention (%)	$R = \left(1 - \frac{c_p}{c_b}\right)\cdot 100$	(8)
OM flux (mgC.m^{-2}.h^{-1})	$J_s = J_v \bullet c_p$	(9)
Estimated parameters		
Mass loss$_{adhesion}$ (%)	$Mass\ loss_{adhesion}, \% = \left(\frac{m_{bypass} - m_{FFFF} - m_p}{m_{bypass}}\right) \bullet 100$	(10)
Permeate drag force (N)	$F_{Dp} = 3\cdot\pi\cdot\eta\cdot d_e\cdot U_p$	(11)
Electrostatic force (N)	$32\cdot\pi\cdot\varepsilon_0\cdot\varepsilon_r\cdot\kappa\cdot d_e\left(\frac{k\cdot T}{2}\right)^2\cdot tan\left(\frac{e\cdot\Psi_p}{4\cdot k\cdot T}\right)\cdot tan\left(\frac{e\cdot\Psi_m}{4\cdot k\cdot T}\right)e^{-\kappa(2\cdot l - d_e)/2}$	(12)

Term	Unit	Definition
A	–	Peak area under the OM peak in the sample runs through the channel with a membrane.
A_0	–	Peak area (−) of OM in the calibration run through a capillary bypassing the channel.
X		OM peak recovery (%) value under normalization to 0–100% for a membrane.
X_{min}		Lowest value of OM peak recovery (%) observed for a given membrane.
X_{max}		Highest value of OM peak recovery (%) observed for a given membrane.
t_0	min	Void time of the unretained sample during focusing.
t_R	min	Retention time (min) of the OM peak during the elution (only the peak closest to the void peak is presented).
Δt	min	t_2-t_1, where t_1 and t_2 (min) are the maxima of peak 1 and peak 2 under consideration.
σ_1	min	$2\sigma_1$ and $2\sigma_2$ are the full width at half maximum (FWHM) of peaks 1 and 2.
c_p	mgC.L^{-1}	Initial permeate concentration, measured using TOC.
c_b	mgC.L^{-1}	Concentration of OM in the cell. The c_{bi} of the *i*th sample was estimated by subtracting the permeate sample concentration, c_{pi}, from the initial feed concentration, c_f, and then dividing it with the corresponding retentate volume, V_{ri}.
J_v	L.m^{-2}.h^{-1}	Flux.
m_{bypass}	mgC	Total OM mass estimated by injecting feed in FFFF-OCD, through a capillary tube bypassing FFFF channel-membrane
m_{FFFF}	mgC	Total OM mass (sum of OM sample peak (peak 1) and reversible OM by permeation (peak 2)) after eluting through the FFFF channel with the membrane.
m_p	mgC	OM mass permeating through membrane in FFFF, estimated by re-injecting the permeate volume in a separate run in FFFF-OCD bypassing the membrane
η	kg.m^{-1}.s^{-1}	Mobile phase viscosity.
d_e	m	Equivalent-volume diameter: diameter of a spherical particle with the same volume as the non-spherical particle.
U_p	m.s^{-1}	Applied permeate flow velocity.
ε_0	C.V^{-1}.m^{-1}	Permittivity of the vacuum.
ε_r	–	Relative permittivity of the solution.
k	kg.m^2.s^{-2}.K^{-1}	Boltzmann constant.
T	K	Absolute temperature.
e	C	Electronic charge.
κ^{-1}	m^{-1}	Debye screening length.
ψ_m, ψ_p	V	Membrane and particle surface electric potentials.
l	m	Mean layer thickness or the position of the particle with respect to the membrane.

2.7. Error analysis

The methodology used to calculate errors in the analysis involves identifying sources of errors, such as temperature variation, permeate flow rate, TOC calibration, and feed preparation by the operator. Membrane originated errors such as the variability in pore size, due to a potentially wider pore size distribution, were accounted for in the error estimation of the membranes' permeability. Absolute errors for measured quantities were calculated using the error propagation method described by Imbrogno et al. [120]. Tables S10–S13 present detailed, quantified errors to ensure a thorough assessment of uncertainties.

3. Results and discussion

The fractionation performance of the membrane in FFFF depends on several factors, such as OM retention, OM-membrane adhesive interactions, and membrane permeability. High OM retention and low adhesive interactions yield high peak recovery in FFFF, whereas a high permeate flow rate generates high permeate drag for separation, thereby

enhancing peak resolution. Peak recovery, resolution, and retention ratio were used as OM fractionation performance indicators to evaluate the different nanofiltration (NF) membranes in FFFF.

3.1. Peak recovery of organic matter during fractionation in FFFF

Evaluating peak recovery in FFFF helps the optimization of OM fractionation when varying membrane material and MWCO, permeate flow rate flow, and mobile phase composition [121]. The peak recovery of various OM types in FFFF was analyzed to examine the loss of OM fractions when different NF membranes were used (Fig. 3A). The apparent MW observed from LC-OCD measurements [122] (see Table S3) is presented to account for the OM size-based peak recovery. A poor peak recovery indicates low retention and high loss of OM fractions by permeation, membrane-OM interactions, or both. The peak recovery of PSS was analyzed to evaluate the fractionation of OM with a range of known molecular weights and the NF membranes under consideration. PSS of MWs 1–280 kDa were selected as model compounds with the same functional group but different sizes (Fig. 3B).

Peak recovery for all membranes was generally high (≥50%) for OMs with a higher carboxylic acidity. AUS, HA, and BSA with carboxylic acidities of 5.2, 7.5, and 9.3 mmol.gC^{-1} exhibited high peak recovery, whereas TAN, TEA, FP, and TA with lower carboxylic acidity exhibited low peak recovery. The retention of negatively charged organic solutes on negatively charged nanofiltration membranes is mainly due to electrostatic repulsion, which prevents the solutes from passing through the membrane. This repulsion, caused by the Donnan effect, is stronger at higher pH levels where the membrane's negative charge is more prominent [6]. As all the membranes (Table 1) have negative surface charges at the filtration pH conditions, the electrostatic repulsion of the OM by the membrane surface is the reason for the high peak recovery of OM with high carboxylic acidity. A similarly high peak recovery (>90%) has been reported for carboxylated polystyrene nanoparticles (85 nm) due to electrostatic repulsion with a negatively charged 30 kDa regenerated cellulose membrane, in contrast to uncarboxylated nanoparticles (102 nm) [123].

High peak recovery is expected when the membrane achieves high OM retention due to size exclusion, charge repulsion, or a combination thereof, and low membrane-OM adhesion [124]. However, despite having the highest net anionic charge of 215 μeq.L^{-1}, high carboxylic acidity of 10 mmol.gC^{-1}, and a high molecular weight of 180 kDa, SA exhibited very poor peak recovery with all membranes compared to HA with an anionic charge of 143 μeq.L^{-1}, carboxylic acidity of 7.5 mmol. gC^{-1}, and a MW of 780 Da (Table S3). Equally important is that the peak recovery did not follow the order of the different OM types' MW (Fig. 3A). This indicates that Donnan exclusion due to identical charges and size exclusion may not be the only factors determining the peak recovery of OM. A synergistic effect of size and charge exclusions, membrane-OM interactions, and drag force may play a role in determining peak recovery [78,124].

Peak recovery of PSS (Fig. 3B) does not strictly follow the order of membrane MWCO, similar to the case of OM (Fig. 3A), even though it is expected to decrease with membrane MWCO [47,54]. Peak recovery of high molecular weight PSS (140 and 280 kDa) is counterintuitively low. A decreased peak recovery for OM is usually observed when i) the membrane-OM adhesion is very high [70,125], ii) OM loss through the permeate is high [47,124], and iii) the permeate drag force is high due to the high permeate flow rate of the membrane and solute with a large molecular size [70,124]. In the first case, PSS with different MWs possess the same functional groups and negative charges. Therefore, the adhesive interactions based on charge and secondary interactions [92] with the membrane would be similar for all PSS irrespective of the MWs, which will not alter the peak recovery. In the second case, the MWCO of all the membranes except HY10 lies below the molecular weight of PSS. Thus, the chances of PSS loss through the permeate are low as the size exclusion works well, in addition to the effect of the Donnan exclusion. Therefore, the decreased peak recovery of PSSs with high molecular weights (67–280 kDa) could be due to the third case: drag forces induced by the larger size of the solute and the resulting drag of OM towards the membrane. A later section explores membrane-OM adhesive interactions and the drag force experienced by OM to evaluate their role in determining OM fractionation.

Evaluating the OM retention of the membrane can help to explain the role of membrane-OM interplay in fractionation [124]. For this, the NF membranes used in FFFF were evaluated in terms of OM retention, OM permeate concentration, and solute flux in stirred cell dead-end filtration at a controlled flux (54 ± 10 L.m^{-2}.h^{-1}) (Fig. 4). The selected flux is comparable to that used in FFFF during the elution of OM.

All OM types except FP were retained over 90%. Among all the membranes, NF270 and NF90 had the highest retention (≥97%) for all OM types except FP, which is one of the smallest. The retention of most of the OM is due to the combined effects of the size-exclusion and Donnan exclusion mechanisms. The size-exclusion mechanism is mostly prevalent for high molecular weight OM, whereas the interplay between size and Donnan exclusion plays a major role in the retention of charged low molecular weight OM [6]. For FP, NF90 exhibited the highest

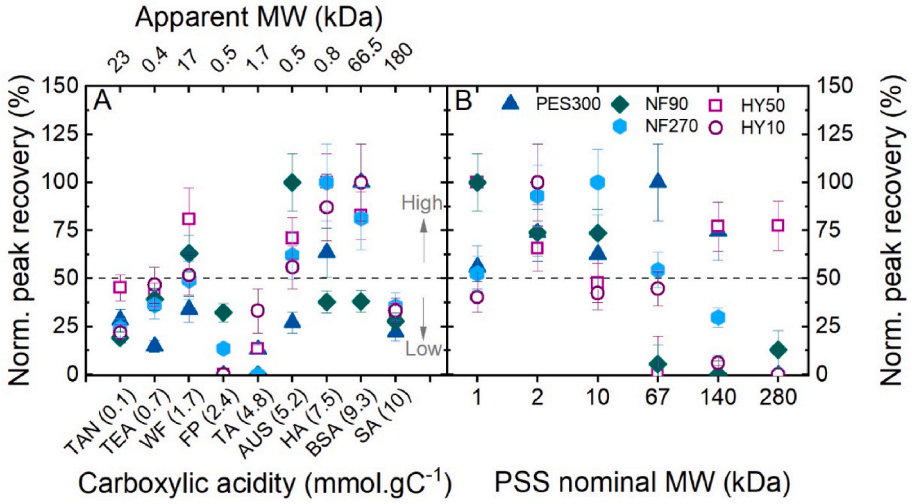

Fig. 3. Peak recovery in FFFF with different NF membranes as a function of (A) OM carboxylic acidity and (B) PSS nominal MW. 15 ± 2 mgC.L^{-1} OM and PSS, 50 μL in 1 mM $NaHCO_3$ and 10 mM NaCl (pH 8.0 ± 0.2), 1 mM KH_2PO_4 and Na_2HPO_4 buffer mobile phase, pH 6.9 ± 0.2, 25 °C, Q_p 3.0 mL.min^{-1}, Q_c 0.5 mL.min^{-1}. High and low peak recovery are differentiated by an arbitrary line at 50%. The normalization indicates the relative peak recovery of OM type for a given membrane.

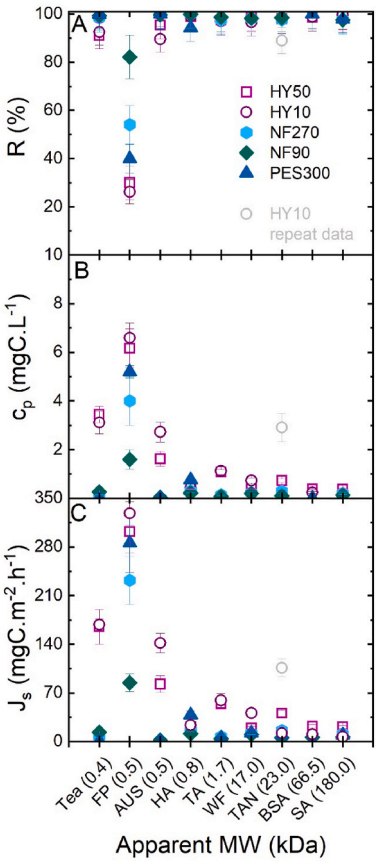

Fig. 4. Organic matter (A) retention, (B) permeate concentration, and (C) solute flux as a function of OM and membrane type during stirred cell NF experiments (13 ± 3 mgC.L^{-1} OM, 700 mL, 1 mM $NaHCO_3$, 10 mM NaCl, pH 8.0 ± 0.2, retention at 65 ± 5% recovery, 400 rpm, 22 ± 1 °C, fixed flux of 54 L.m^{-2}.h^{-1}, membrane area 38.5 cm^2).

retention of 82%, NF270 had a mid-range retention of 54%, and HY10 had the lowest retention of 26%. The highest permeate concentration of 6.6 mgC.L^{-1} was observed for FP with HY10. The poor FP retention was a result of poor size exclusion due to the larger pore diameter (~1.4 nm) of HY10 in comparison to the hydrodynamic diameter of FP (~0.5 nm). Additionally, poor charge repulsion due to a relatively weaker zeta potential of HY10 (−38 mV) and FP's very low anionic charge (2 μeq.L^{-1}) led to HY10's poor retention of FP. A decrease in the permeate concentration of OM with apparent molecular weight is evident in Fig. 4B. The most extensive variation in OM retention and OM flux for different OM types was observed for the membranes HY10 and HY50, whereas NF90, NF270, and PES300 membranes showed very similar OM retention and flux, except for FP.

Permeate OM concentration and solute flux decreased with the apparent molecular weight of the OM. On the other hand, the peak recovery observed in FFFF (Fig. 3) did not show any trend with respect to the apparent molecular weight of OM. Even though peak recovery obtained by OM elution in FFFF is broadly analogous to the retention obtained by OM filtration in the stirred cell, the different trends between OM peak recovery in FFFF (Fig. 3) and OM retention in stirred cells (Fig. 4) imply that OM-membrane adhesive interactions (electrostatic, van der Waals and hydrophobic) other than size exclusion play a role in OM fractionation in FFFF. It should be noted that the FFFF process differs greatly from NF filtration in a stirred cell, which hinders direct comparison.

The OM peak resolution and peak retention ratio were evaluated further to understand the role of each membrane in separating the OM fractions.

3.2. Separation of OM fractions: peak retention ratio and peak resolution

The fractionation of OM types with low molecular weight fractions (e.g., TEA, FP, and TA) is challenging, perhaps due to their low peak recovery, faster diffusion, and low drag force. The fractionation of OM types with larger fractions (e.g., TAN and SA) is equally challenging, possibly due to their enhanced interactions with the membrane because of greater proximity to the membrane surface induced by the high permeate drag force. The peak retention ratio and resolution of the smallest fractions resolved for OM (peaks eluting nearest to the void peak) are presented for evaluating the fractionation of OM with different NF membranes (Fig. 5).

The peak resolution of OM fractions (Fig. 5A) did not vary with different membranes and OM types except for HA and BSA. On the other hand, the peak resolution of PSS (Fig. 5B) improved with nominal molecular weight. Different NF membranes did not have a considerable impact on the peak resolution of low molecular weight PSS (1–10 kDa) compared to high molecular weight PSS (67–280 kDa). NF90 and NF270 had the highest peak resolution for all PSS fractions.

HA, with a carboxylic acidity of 9.3 mmol.gC^{-1}, exhibited an optimal peak retention ratio of 0.25 (designated by Gigault *et el.* [126]) with NF270 and a moderate peak retention ratio of 0.55 with NF90. BSA with high carboxylic acidities of 7.5 mmol.gC^{-1} also showed a moderate peak retention ratio. However, AUS and SA with carboxylic acidities of 5.2 and 10 mmol.gC^{-1} did not exhibit low peak retention ratios. Similarly, other OM types exhibited poor peak retention ratios (0.6–1.0) across all membranes (Fig. 5C).

An increase in peak retention ratio corresponding with PSS's molecular weight was very evident for all membranes (Fig. 5D). High molecular weight PSS (67–280 kDa) had excellent peak retention ratios (≤0.3) (Fig. 5D) and good separation with all membranes compared to low molecular weight PSS (≤10 kDa). This observation is in agreement with previous reports [47,127] that the peak retention ratio reduces (separation enhances) with the molecular weight of the solute. For instance, the 10 kDa PSS was observed to have a peak retention ratio of 0.6, whereas it was 0.3 for the 30 kDa PSS when fractionated with a 1 kDa MWCO UF membrane [47]. The peak retention ratio significantly improved when using an NF membrane in comparison with UF membranes. In previous work [47], a UF membrane with a 1 kDa MWCO at a permeate flow rate of 2.0 mL.min^{-1} resulted in a peak retention ratio of 0.6. However, using NF membranes with a 0.3 kDa MWCO at a permeate flow rate of 3.0 mL.min^{-1} improved the peak retention ratio to 0.3, indicating the higher efficiency of NF membranes in fractionating OM in the lower molecular weight range.

The solution's ionic strength affects charge repulsion and may cause a difference in peak resolution and retention ratio. In nanofiltration, the feed solution's ionic strength affects separation, while in FFFF, the mobile phase ionic strength is important as only a small sample volume of 50 μL is injected into a continuously flowing mobile phase in the channel with a channel volume of 700 μL.

3.3. The role of ionic strength in improving fractionation

The solution's ionic strength can influence the OM-membrane interaction in several ways: i) the ability of a negatively charged OM to approach or pass through the membrane increases at high ionic strength due to the reduction in electrostatic double layer thickness [128], ii) structural changes in the membrane due to a thinning of the double layer can lead to reduced water permeability [129], and iii) conformational changes of the OM such as coiling or aggregation can lead to an increase or decrease in OM retention [47,51]. In addition, when a membrane's salt retention is high, a counteracting osmotic pressure will reduce the effective driving force created by the applied permeate flow. Thus, peak recovery of OM may reduce with ionic strength due to its adhesion to the membrane or permeation through the membrane [47,125]. These fractionation characteristics, such as peak

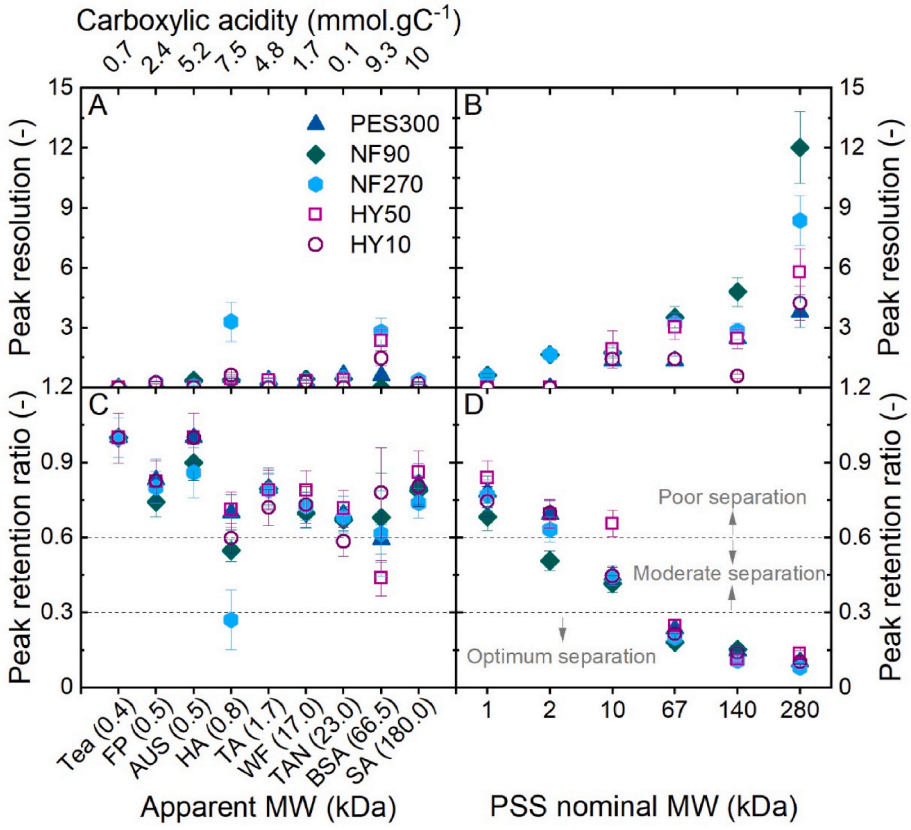

Fig. 5. Peak resolution and peak retention ratio of OM (A, C) and PSS (B, D) in FFFF with different NF membranes. 15 ± 2 mgC.L^{-1} OM, 50 μL, pH 8.0 ± 0.2 in 1 mM $NaHCO_3$ and 10 mM NaCl, 1 mM KH_2PO_4 and Na_2HPO_4 buffer mobile phase, pH 6.9 ± 0.2, 25 °C. Qp 3.0 mL.min^{-1}, Qc 0.5 mL.min^{-1}. Peak resolution and peak retention ratio are presented for the smallest resolved OM fraction nearest to its void peak.

recovery and peak resolution at various ionic strengths, could potentially be used to assess how fractionation is affected by membrane-solute interactions.

SA, HA, and FP were selected for ionic strength experiments based on carboxylic acidity, anionic charge, and size (see Table S3). Among the OM types studied, SA is the largest, with a molecular weight of 180 kDa, high carboxylic acidity of 10 mmol.gC^{-1}, and a high net anionic charge of 218 μeq.L^{-1}. HA is one of the most widely studied OM types for fractionation (Table S2), with a small size of 0.8 kDa, high carboxylic acidity of 7.5 mmol.gC^{-1}, and a moderate net anionic charge of 143 μeq.L^{-1}. FP is one of the smallest OM types, with a size of 0.5 kDa, low carboxylic acidity of 2.4 mmol.gC^{-1}, and a poor net anionic charge of 2 μeq.L^{-1}. Three membranes HY10, NF270, and PES300 were selected for the ionic strength experiments based on their active layer chemistry (sulfonated polyethersulfone, semi-aromatic piperazine-based polyamide, and polyether sulfone), zeta potential (−38, −55, and −77 mV), MWCO (3, 0.3, and 0.3 kDa), and permeability (54, 16, and 5 L m^{-2}.h^{-1}.bar^{-1}) (see Table 1). The OM fractionation with the selected OM types (SA, HA, and FP with NF270 and HY10) was performed at varying ionic strength (0–100 mM $NaNO_3$) of the mobile phase. Fig. 6 presents the elugrams of fractionation.

At all ionic strengths, NF270 exhibits higher peak intensity and better-defined peaks than PES300 and HY10, which have poor peak intensity and poorly resolved peaks. Prominent signals for FP are not observed with HY10 and PES300, indicating a nearly complete loss of FP through HY10 and possible combined effects of adhesion and loss in the case of PES300. Conversely, FP peaks are present in the case of NF270 but are poorly separated. HA and SA exhibit peaks of smaller intensity with PES300 and HY10 than NF270 at all ionic strengths. Fractionation into partially separated multiple peaks of SA and HA is apparent for NF270 in Fig. 6D and G, whereas PES300 and HY10 did not produce such a multipeak fractionation. The changes observed in the elution profiles at higher mobile phase ionic strengths are due to a shift in the balance between permeate drag force and diffusion, affecting the steady-state cloud of particles [125]. Increasing ionic strength compresses the electrostatic double layer of both the membrane and OM [128], reducing the OM's hydrodynamic diameter. For instance, the hydrodynamic size of PSS has been reported to decrease with ionic strength due to compression of the electrical double layer and collapsed conformation [130]. Such a reduction in the electrostatic double-layer thickness allows OM molecules to move closer to the membrane, potentially leading to increased interaction, irreversible adsorption, and sample loss during fractionation [51,125]. The separation of larger OM fractions is particularly sensitive to changes in ionic strength [125], as larger fractions are more influenced by hydrodynamic drag and electrostatic forces. Increased interactions with the membrane at higher ionic strengths can slow down larger fractions during elution, leading to enhanced separation, as observed in Fig. 6. High ionic strength can also cause aggregation of some solutes, leading to an increase in their hydrodynamic size, which in turn affects their fractionation [51]. The size distribution of HA is reported to be slightly broadened due to aggregation at increased ionic strengths [131,132]. The additional shoulder at 12 min that appeared for HA at 100 mM with NF270 membrane is most likely due to the aggregation of HA at such a high ionic strength.

Fig. 7 presents the impact of ionic strengths on peak recovery, retention ratio, and resolution.

The impact of mobile phase ionic strength on peak retention ratio varied with OM and membrane type. For NF270, the lowest peak retention ratio for HA, SA, and FP was observed at 10 mM mobile phase ionic strength, indicating the highest separation at this intermediate ionic strength. For HY10, the lowest OM peak retention ratio was also observed for the 10 mM $NaNO_3$ condition, except for FP, which was

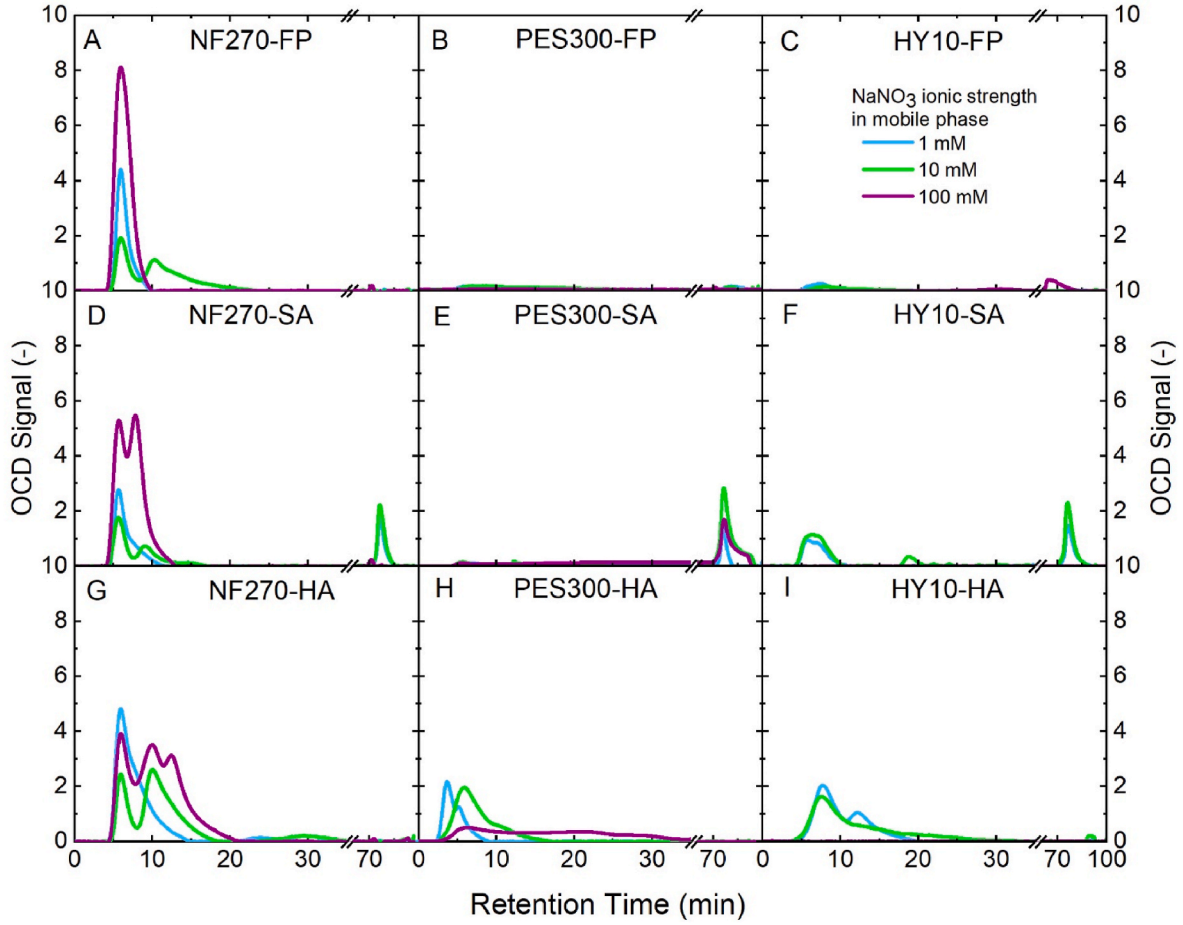

Fig. 6. Elugram of HA, FP, and SA with NF270, PES300 and HY10 membranes at different ionic strengths. 15 ± 2 mgC.L^{-1} OM, pH 8.0 ± 0.2 in 1 mM $NaHCO_3$ and 10 mM NaCl, mobile phase: 0, 10, and 100 mM $NaNO_3$ added to KH_2PO_4 and Na_2HPO_4 1 mM buffer, pH 6.9 ± 0.2, 25 °C, Qp 3.0 mL.min^{-1}, Qc 0.5 mL.min^{-1}. There are no elugrams for HY10 at 100 mM $NaNO_3$ due to the absence of a signal detected in OCD.

completely lost at this ionic strength. At 100 mM $NaNO_3$, all the OM types were lost with HY10, whereas only FP was lost with NF270. On the other hand, PES300 presented very high peak retention ratios indicating a poor retention for all OM at all ionic strengths.

Peak resolution generally deteriorated with ionic strength for NF270 and HY10. At 10 mM $NaNO_3$, slightly improved peak resolution was observed for SA and FP with the NF270 membrane, whereas HA did not exhibit much difference from the 1 mM ionic strength condition. Peak recovery of HA increased when ionic strength was increased to 10 mM with both NF270 and HY10, but such an increase was not evident for SA and FP. However, the complete loss of FP was observed at ionic strengths of 10 and 100 mM. The difference in charge screening and interaction between HA, SA, and FP with the membranes could be the reason for different peak recoveries and peak resolutions for these OM types across different membranes in FFFF. Increasing ionic strength in the solution leads to the compression of the electrical double layer surrounding the negatively charged organic solutes [128] and may also cause solute aggregation in some cases [51]. Larger aggregates are more likely to be retained by the membrane due to size exclusion mechanisms, while smaller aggregates or individual molecules might permeate more readily. The increased peak recovery of HA at high ionic strengths of 10–100 mM is likely due to an increase in its size because of aggregation. On the other hand, SA exhibits such an increase in peak recovery only at 100 mM ionic strength, not at 10 mM. The reduction in or absence of FP peak recovery at high ionic strengths might be due to the loss of FP on the membrane, which can happen due to its adsorption or permeation through the membrane caused by the masking of electrostatic repulsion and compression of the electrical double layer of both the membranes and FP.

Considering only electrostatic interactions, HA and SA are expected to interact similarly with the membrane due to their high carboxylic acidity of 7.5 and 10 mmol.gC^{-1} and substantial net anionic charge of 143 and 218 L.mgC^{-1}.m^{-1}, respectively. However, explanations based on OM-membrane electrostatic interactions are insufficient to explain the fractionation behavior of HA, SA, and FP in response to the change in the mobile phase's ionic strength. The difference in HA and SA elution properties at varying ionic strengths leads to the hypothesis that additional interactions may also play a role in their fractionation.

Multiple factors such as hydrodynamic, electrostatic, and adhesive interactions were examined to validate the hypothesis of distinct interactions of HA, SA, and FP with membranes.

3.4. *Membrane-OM interactions responsible for fractionation*

To verify the hypothesis that the difference in peak resolution and peak retention ratio behaviors of OMs is due to different OM-membrane interactions, the following factors were estimated (Fig. 8) using FFFF elution data based on protocols adapted from previous reports; i) permeate drag force (due to different OM size and membrane permeate flow velocity) [47], ii) electrostatic force (due to different charges of OM and membranes) [47], ii) electrostatic force (due to different OM charges and membranes) [47], OM mass loss due to adhesion to the membrane (due to different functional groups) [92].

As expected, the impact of ionic strength on the mass loss due to adhesion varies with the nature of the OM and membrane. PES300 exhibits the highest mass loss due to adhesion when compared to NF270

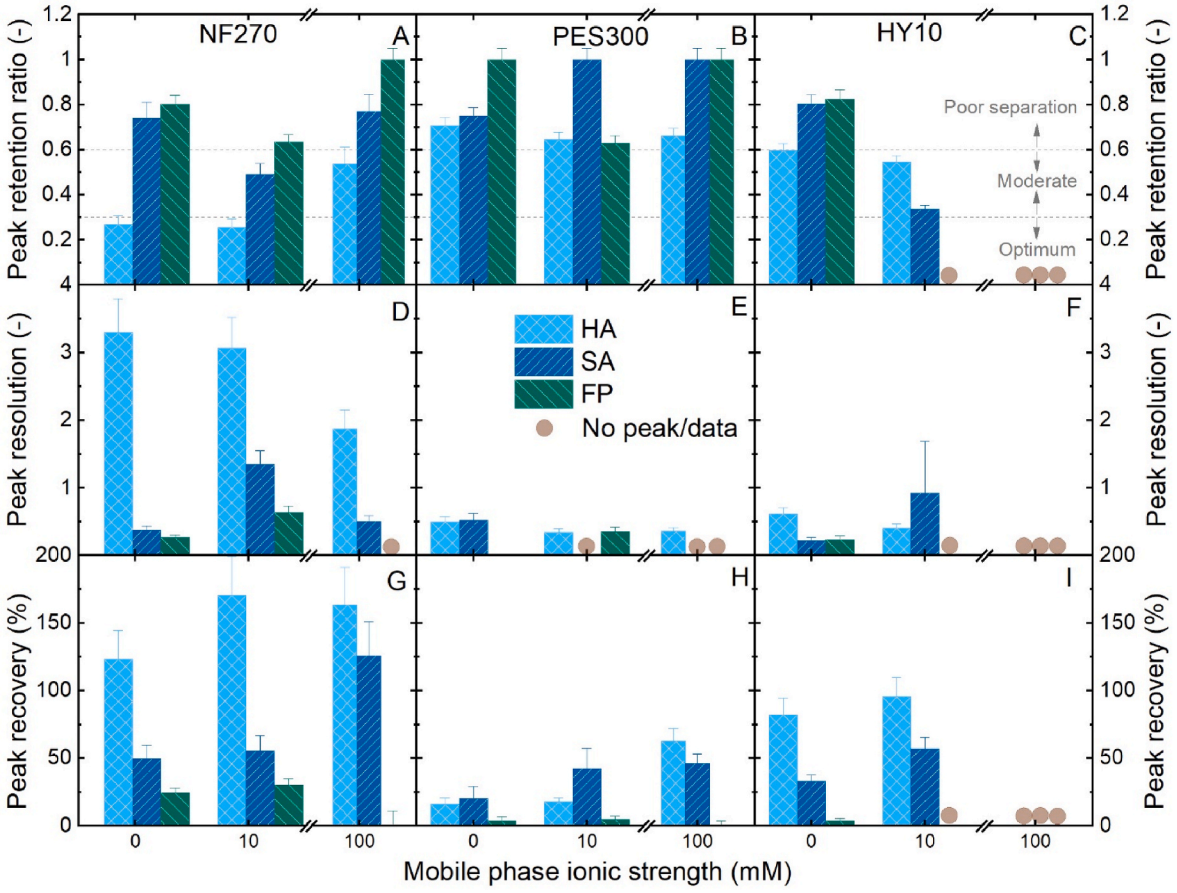

Fig. 7. Peak recovery, retention ratio, and resolution in FFFF of HA, FP, and SA with NF270 (A, D, G), PES300 (B, E, H) and HY10 (C, F, I) membranes at different ionic strengths. 15 ± 2 mgC.L^{-1} OM, pH 8.0 ± 0.2 in 1 mM $NaHCO_3$ and 10 mM NaCl, mobile phase: 0, 10, and 100 mM $NaNO_3$ added to KH_2PO_4 and Na_2HPO_4 1 mM buffer, pH 6.9 ± 0.2, 25 °C, Qp 3.0 mL.min^{-1}, Qc 0.5 mL.min^{-1}. Missing data for 10 and 100 mM $NaNO_3$ are due to the absence of a signal or a poor signal detected in OCD.

and HY10. For NF270, the mass loss of HA and FP due to adhesion did not change with the ionic strength of the mobile phase, in contrast to SA. The mass loss of SA decreased with the ionic strength, supporting the observation of an increase in peak recovery of SA with ionic strength, indicating higher retention of SA with NF270 membranes at high ionic strength. The nearly complete retention (>99%) of SA in stirred cell filtration with the NF270 membrane at 100 mM $NaNO_3$ ionic strength supports this observation of increased peak recovery. For, PES300 the mass loss of both HA and SA decreased with ionic strength, whereas the mass loss of FP was unaffected by ionic strength. Conversely, for HY10, the mass loss of HA, SA, and FP increased with ionic strength. The fact that HA (98%), FP (90%), and SA (99%) are well retained in stirred cell filtration with HY10 membrane at 100 mM $NaNO_3$ suggests that the OM mass lost due to adhesion could be due to deposition on the membrane surface or in the membrane pores.

The permeate drag force for HA, SA, and FP with NF270 increased at an ionic strength of 10 mM and stayed constant with a further increase in ionic strength. The permeate drag force for PES300 did not change considerably for HA and FP, whereas decreased for SA with ionic strength. For HY10, the permeate drag force increased for HA and SA at an ionic strength of 10 mM but did not change for FP. The electrostatic repulsive force diminished with ionic strength for HA and SA for both membranes. The electrostatic repulsive force of FP was not high enough to observe any changes. At 100 mM ionic strength, a major fraction of HA and SA were adhered to HY10 due to the reduction in resistance due to electrostatic repulsion and reduced further, probably due to the reduction in the size of the OM due to coiling [116,133]. The electrostatic repulsive force diminished completely with an increase in ionic strength from 0 to 100 mM. A decrease in electrostatic persistence length from approximately 115 nm–17 nm for SA was observed with a change in ionic strength from 10 to 100 mM [134]. A decrease in electrostatic persistence length leads to a decrease in the overall stiffness of the polymer chain. Consequently, the polymer chain becomes more flexible and less extended. Additionally, the same study found that the electrostatic repulsions between the SA chains are screened at a distance of approximately 100 nm. This observation is in qualitative agreement with the observation of poor or no electrostatic forces (F_E) at an ionic strength ≥10 mM at a distance of 10 nm used to estimate F_E. A compact and more flexible conformation of SA may result in increased adhesive interactions or even deposition on the surface and pores of the HY10 membrane. Such a change in mass loss or permeate drag force was not observed for PES300 with lower permeability and smaller pores.

The results indicate that OM-membrane interactions depend on OM and membrane properties. The high adhesive interaction and permeate drag of SA might be responsible for its poor peak resolution and retention ratio, especially with HY10, even though the electrostatic repulsion of SA is higher than HA. The results for FP suggest that if the OM is not charged and adhesive interaction with the membrane is high, peak recovery and peak resolution can be low. This means fractionation depends on the OM size, charge, and adhesive interactions when using NF membranes. For instance, a membrane such as NF270 with a high negative surface charge, moderate pure water permeability, and a low MWCO may be used with moderate ionic strength (e.g., 10 mM NaCl) for the fractionation of HA.

Given the minimal or conditional differences observed in the fractionation of various OM types, applying the method to a mixture of these

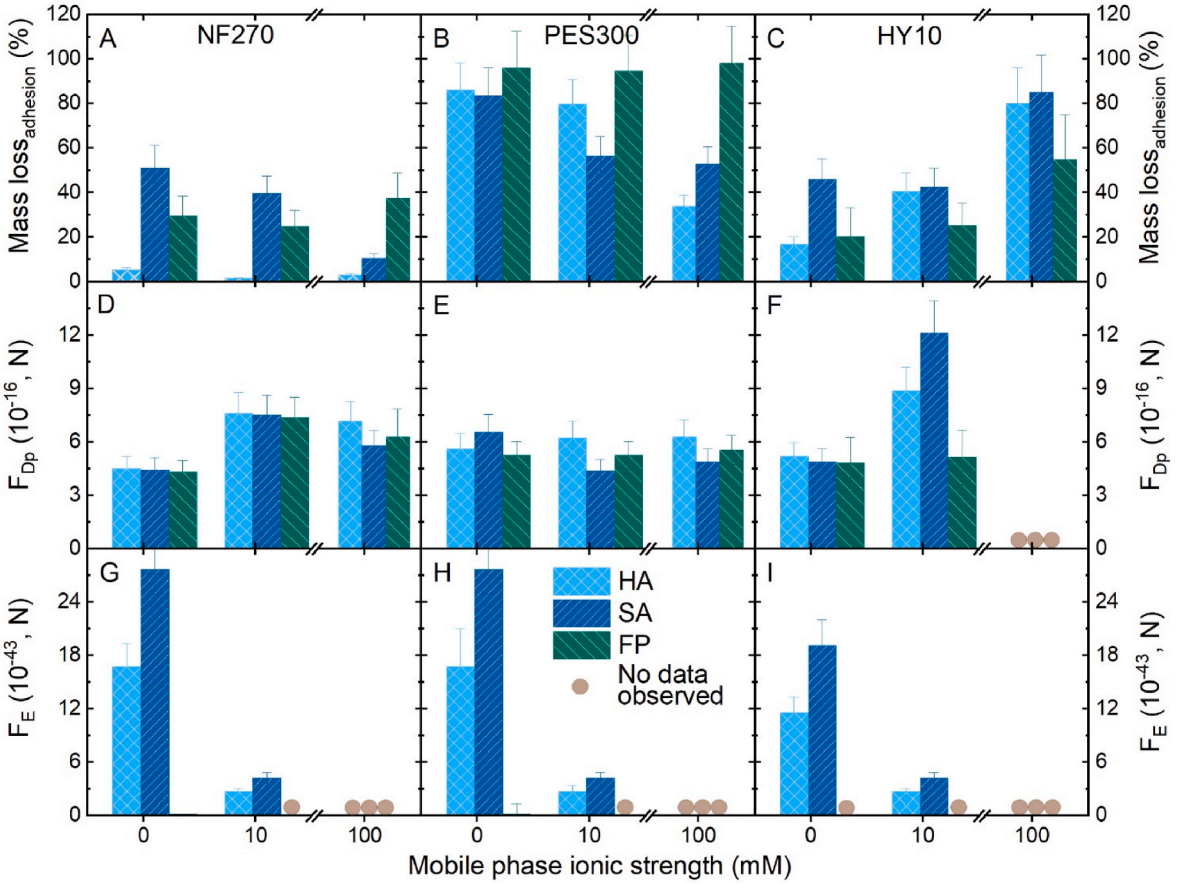

Fig. 8. OM mass loss due to adhesion, permeate drag force (F_{Dp}), and electrostatic forces (F_E) with NF270, PES300 and HY10. F_E was calculated at a membrane-OM distance of 10 nm. 15 ± 2 mgC.L^{-1} OM, pH 8.0 ± 0.2 in 1 mM $NaHCO_3$ and 10 mM NaCl, mobile phase: 0, 10, and 100 mM $NaNO_3$ added to KH_2PO_4 and Na_2HPO_4 1 mM buffer, pH 6.9 ± 0.2, 25 °C. The missing data points for F_{Dp} and F_E are due to the absence of observable signals.

OM types is justified as it better represents the complex and heterogeneous nature of OM in real water environments. This approach enhances the relevance and applicability of the findings to real-world scenarios where mixtures of different OM types are commonly encountered.

3.5. Fractionation of natural organic matter

The fractionation of a mixture of nine different OM types, namely HA, AUS, FP, SA, WF, TA, TAN, TEA, and BSA, with a net TOC of 36 mgC.L^{-1}, was performed at different ionic strengths with NF270 and HY10 to evaluate the suitability of NF to fractionate a complex model matrix of OM. Additionally, NOM fractionation was carried out using surface water samples from rivers, lakes, swamps, and wastewater sources (Fig. 9). The organic carbon and organic nitrogen fractions present in the samples, analyzed using LC-OCD-OND are presented in Fig. S15. The diverse water types offer a broad basis for evaluating the FFFF method's effectiveness in fractionating water samples with varying NOM characteristics.

The elugram of the mixture of nine OM types shows a distribution of multiple peaks at various retention times. NF270 exhibits higher peak intensity (height) and fractionation than PES300 and HY10 for all conditions. Elugrams with a normalized peak height for comparison of the peak profile are provided in Fig. S14. The peak positions of the OM mix sample do not strictly match the peak retention times of its components when fractionated independently. Similar observations were reported for various molecular weights using a 0.3 kDa MWCO membrane [135]. Peak intensity and, hence, peak recovery are highest at very low ionic strength in the absence of $NaNO_3$, in contrast to the individual OM runs. Peak recovery of the OM mixture at 100 mM $NaNO_3$ is very low, presumably due to the loss of OM due to adhesion and permeation, as in the case of individual OM fractionations (Fig. 7).

The surface water samples generally exhibit multiple peaks and broader distributions, indicating complex mixtures of NOM with varying molecular sizes. Peak shoulders and multiple peaks are more pronounced with NF270 than PES300 and HY10, indicating that NF270 provides better separation of heterogeneous NOM fractions. All the surface water samples display multiple peaks and shoulders on the NF270 membrane at 0 and 10 mM ionic strength, indicating a diverse NOM composition. The natural water samples exhibit broader peaks and more shoulders than HA, suggesting a more heterogeneous NOM. The OM mix sample shows distinct peaks with shoulders, similar to the profiles observed in the natural water samples at a low retention time (low molecular weight region). At a low ionic strength of 0 mM, all samples exhibit broad peaks with multiple shoulders, indicating high NOM heterogeneity. At a medium ionic strength of 10 mM, peaks become slightly more defined, showing a mix of NOM fractions. At 100 mM, peaks are narrower or absent, indicating a substantial loss in the information on NOM fractions, especially with PES300 and HY10 membranes. While the loss of NOM in HY10 is attributed primarily to permeation, the case of PES300 suggests a synergistic effect of both permeation and adhesive interactions, as observed with various types of OM (Fig. 8).

A 0.3 kDa MWCO NF membrane with lower OM interaction proved superior to both a 0.3 kDa MWCO membrane with higher OM interaction and a 3 kDa membrane with high OM loss for fractionating NOM, as it offers better separation of heterogeneous NOM fractions. This study advances previous findings by offering detailed evidence supporting the use of NF membranes for better size fractionation, consistent with earlier

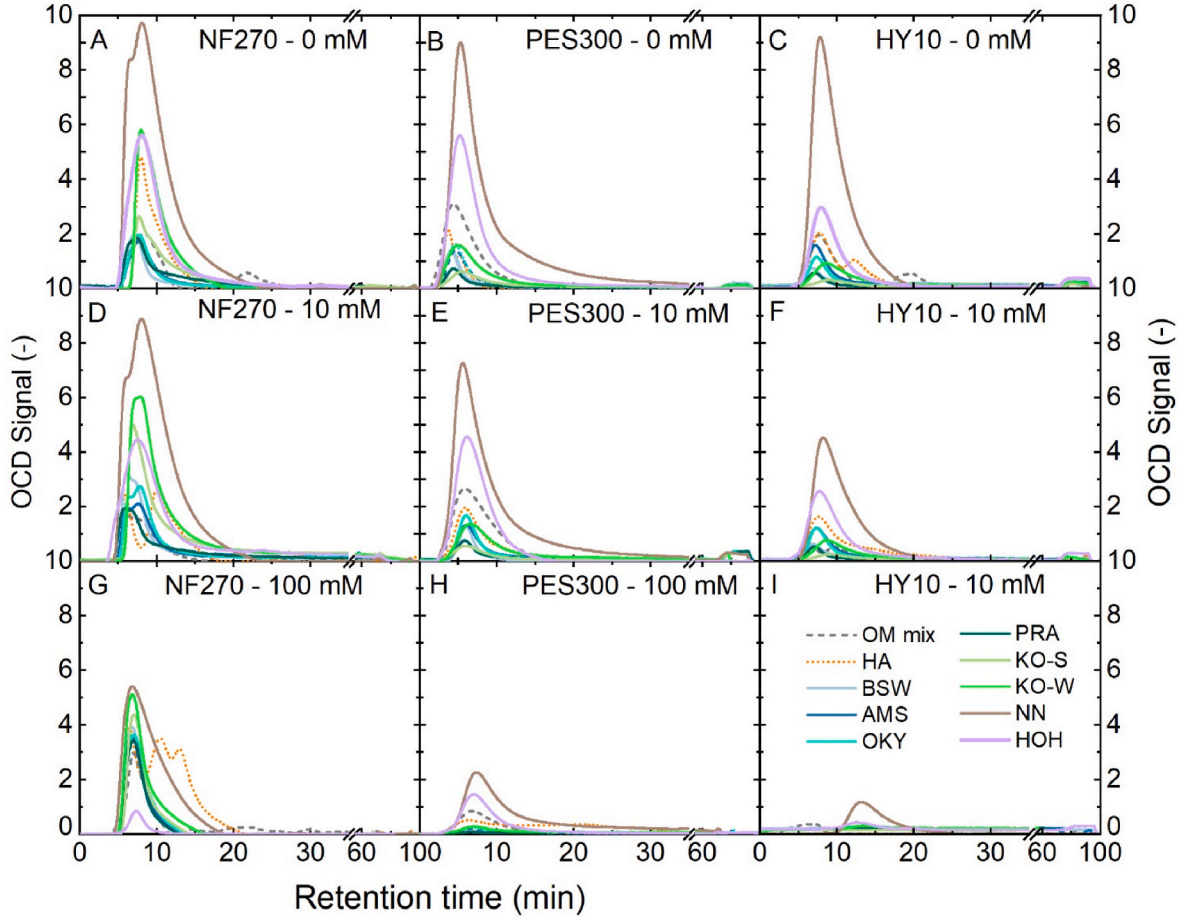

Fig. 9. Elugrams of OM mix (mixture of HA, AUS, FP, SA, WF, TA, TAN, TEA, and BSA with a net TOC of 36 mgC.L^{-1}) in 1 mM $NaHCO_3$ and 10 mM NaCl at pH 8.0 ± 0.2, and surface water samples from Germany (HOH: Hohloch Swamp Lake), Ghana (BSW: Bosumtwe lake, AMS: Amansuri Lake, OKY: Okye River, PRA: Pra River), The Gambia (KO–S: Kotu stream, KO–W: Kotu wastewater), and Tanzania (NN: Ngare Nanyuki Swamp) with NF270, PES300 and HY10 membranes at different ionic strengths of mobile phase: A–C) 0 mM; D–F) 10 mM; and G-I) 100 mM $NaNO_3$ added to KH_2PO_4 and Na_2HPO_4 1 mM buffer, pH 6.9 ± 0.2, 25 °C, Qp 3.0 mL.min^{-1}, Qc 0.5 mL.min^{-1}. HA (15 mgC.L^{-1}) is presented as a reference.

reports [52,54] recommending colloidal size characterization of natural DOM samples using 0.3 kDa MWCO membranes using FFFF coupled with UV/fluorescence detectors. OCD coupled with FFFF enables the fractionation of OM fractions that are not UV/fluorescence active. However, the long capillary connections used in this setup can decrease peak resolution due to OM diffusion within the tubing.

In the low molecular weight range, LC-OCD with an SEC column outperforms FFFF with NF membranes for the separation of different OM fractions (see Fig. S15). Therefore, it is essential to focus on improving NF-based FFFF to enhance their performance in these applications. The NF membrane-based fractionation of OM demonstrates that peak recovery, retention ratio, and peak resolution of many organic compounds can be improved by choosing a membrane with a low MWCO such as 0.3 kDa, and by adjusting the salt concentration of the mobile phase typically to moderate ionic strength. NF remains limited by the permeability, which raises incompatibility issues with the commercial FFFF channel hardware. The pressure limitations of the FFFF channel can be overcome, similar to ultra-high pressure chromatography, when suitable pumps that can deliver constant permeate flow without fluctuations are employed. The range of NF membranes for fractionation can then be further improved to achieve size fractionation at the lower limit, enabling enhanced separation of OM fractions in the 500 Da size range. A challenge that will not be so simple to resolve is the interference in OM signal intensity and size distribution caused by salt retention by denser NF membranes.

4. Conclusions

Five nanofiltration (NF) membranes of varying MWCOs and material compositions were applied in FFFF to assess the fractionation efficiency of humics, polyphenols, biopolymers, and low molecular weight organics. The impact of NF membranes on the fractionation of nine OM types in FFFF was evaluated in terms of peak recovery, peak resolution, and peak retention ratio. The influence of varying ionic strength on peak recovery and resolution of OM was assessed, and the contribution of electrostatic, adhesive, and permeate drag interactions between OM and NF membranes in fractionation at different ionic strengths in FFFF was estimated.

The fractionation of OM in FFFF is governed not only by the MWCO of the membrane but also by the OM-membrane interactions. Peak recovery of the OM in FFFF depends on factors such as the electrostatic and adhesive interactions between the membrane and OM and the permeate drag, in addition to the size exclusion. Stirred cell filtration of OM was conducted with the same membranes used in FFFF to perform a

detailed analysis of peak recovery and solute flux.

NF membrane with a MWCO of 0.3 kDa and low OM interaction exhibited notably good peak recovery and peak resolution for OM types such as HA. Conversely, a loose NF membrane with an MWCO of 3 kDa demonstrated poor peak recovery, attributed to significant OM loss resulting from both adhesion and permeation, particularly at high ionic strengths (100 mM). A 0.3 kDa NF membrane (NF270) at low ionic strength demonstrated effective fractionation of a diverse mixture of nine types of OM, and NOM in surface water samples from rivers, swamps, and lakes across four different countries. In line with previous studies that suggested colloidal size characterization of natural DOM samples, this work expands on prior findings by providing extensive evidence supporting the use of NF membranes for improved size fractionation.

The capability of NF membranes to analyze OM and colloids in the smallest size range ($\leq$1 kDa MW) can be enhanced by selecting an appropriate mobile phase composition, such as low to moderate ionic strength, and by modifying the surface characteristics of the active layer to control OM interaction. Addressing pressure limitations within FFFF channel hardware will be a critical step in advancing the application of NF membranes for fractionating low molecular weight OM fractions.

CRediT authorship contribution statement

Akhil Gopalakrishnan: Writing – original draft, Supervision, Methodology, Investigation, Formal analysis, Data curation, Conceptualization. **Susan Treasa:** Writing – review & editing, Investigation, Data curation. **Youssef-Amine Boussouga:** Writing – review & editing, Supervision, Methodology, Formal analysis, Conceptualization. **Andrea I. Schäfer:** Writing – review & editing, Supervision, Resources, Project administration, Methodology, Funding acquisition, Conceptualization.

Declaration of competing interest

The authors declare that they have no known competing financial interests or personal relationships that could have appeared to influence the work reported in this paper.

Data availability

Data will be made available on request.

Acknowledgments

Helmholtz Association Recruitment initiative is thanked for funding IAMT. Membranes were supplied by Millipore and Nitto Hydranautics. HeiKa is thanked for the HeiKa Explore project funding. The BMBF-supported project CANDECT (BMBF IGSTC call 2015) funded the procurement of the FFFF instrument, with supplementary support provided by RealMethod project funding. DFG funded water sampling in Ghana under the scheme DFG-Kooperation mit Subsahara-Afrika 2020: IIC–Solar Energy; Francis Adu-Boahene (IAMT) and Martin Ansong (IMT) assisted with Ghana water sampling. Prof. Dr. Bryce S. Richards (IMT) assisted with water sampling in Ghana and Tanzania and collected water samples from Kotu in The Gambia. Lamin Fadera from the Gambia National Water & Electric Company (NAMWEC) provided valuable information on the Kotu WWTP, The Gambia. Dr. Minh Nguyen and James Joseph (IAMT) performed OND instrument calibration. Dr. Majda Breida (IAMT) performed 20 NF filtration experiments with HY10 and HY50 membranes, a part of OCD-OND analysis and provided SUVA estimation for the supporting information. Nurul Faiqotul Himma and Dr. Yanghui Cai (IAMT) assisted with zeta potential and TOC measurements. Prof. Dr. Erwin Klumpp, Forschungszentrum Jülich, Germany, is thanked for the inspiration for FFFF-OCD coupling.

Appendix A. Supplementary data

Supplementary data to this article can be found online at https://doi.org/10.1016/j.memsci.2024.123248.

References

[1] V. Artifon, E. Zanardi-Lamardo, G. Fillmann, Aquatic organic matter: Classification and interaction with organic microcontaminants, Sci. Total Environ. 649 (2019) 1620–1635.
[2] J.-P. Croué, Isolation of humic and non-humic NOM fractions: structural characterization, Environ. Monit. Assess. 92 (2004) 193–207.
[3] I.H. Suffet, P. Maccarthy, Introduction, in: I.H. Suffet, P. Maccarthy (Eds.), Aquatic Humic Substances: Influence on Fate and Treatment of Pollutants, American Chemical Society, Washington, DC, 1988 xiii-xxx.
[4] E.M. Perdue, Chemical composition, structure, and metal binding properties, in: D.O. Hessen, L.J. Tranvik (Eds.), Aquatic Humic Substances: Ecology and Biogeochemistry, Springer-Verlag Berlin Heidelberg GmbH, Heidelberg, 1998, pp. 41–61.
[5] M. Sillanpää, Y. Park, Chapter 1 - general introduction, in: M. Sillanpää, Y. Park (Eds.), Natural Organic Matter in Water, second ed., Butterworth-Heinemann, 2023, pp. 1–17.
[6] D.S. Mallya, S. Abdikheibari, L.F. Dumée, S. Muthukumaran, W. Lei, K. Baskaran, Removal of natural organic matter from surface water sources by nanofiltration and surface engineering membranes for fouling mitigation – a review, Chemosphere 321 (2023) 138070.
[7] G.R. Aiken, H. Hsu-Kim, J.N. Ryan, Influence of dissolved organic matter on the environmental fate of metals, nanoparticles, and colloids, Environ. Sci. Technol. 45 (2011) 3196–3201.
[8] C.C. Blanchet, C. Arzel, A. Davranche, K.K. Kahilainen, J. Secondi, S. Taipale, H. Lindberg, J. Loehr, S. Manninen-Johansen, J. Sundell, M. Maanan, P. Nummi, Ecology and extent of freshwater browning - what we know and what should be studied next in the context of global change, Sci. Total Environ. 812 (2022) 152420.
[9] X. Chen, J. Wang, H. Wu, Z. Zhu, J. Zhou, H. Guo, Trade-off effect of dissolved organic matter on degradation and transformation of micropollutants: a review in water decontamination, J. Hazard Mater. 450 (2023) 130996.
[10] L.A. Seders Dietrich, D.P. McInnis, D. Bolster, P.A. Maurice, Effect of polydispersity on natural organic matter transport, Water Res. 47 (2013) 2231–2240.
[11] M.A. Schlautman, J.J. Morgan, Effects of aqueous chemistry on the binding of polycyclic aromatic hydrocarbons by dissolved humic materials, Environ. Sci. Technol. 27 (1993) 961–969.
[12] A. Hartland, I.J. Fairchild, J.R. Lead, H. Zhang, M. Baalousha, Size, speciation and lability of NOM–metal complexes in hyperalkaline cave dripwater, Geochim. Cosmochim. Acta 75 (2011) 7533–7551.
[13] A. Riyadh, N.M. Peleato, Natural organic matter character in drinking water distribution systems: a review of impacts on water quality and characterization techniques, Water 16 (2024) 446.
[14] I. Owusu-Agyeman, M. Reinwald, A. Jeihanipour, A.I. Schäfer, Removal of fluoride and natural organic matter from natural tropical brackish waters by nanofiltration/reverse osmosis with varying water chemistry, Chemosphere 217 (2019) 47–58.
[15] S. Meylan, F. Hammes, J. Traber, E. Salhi, U. von Gunten, W. Pronk, Permeability of low molecular weight organics through nanofiltration membranes, Water Res. 41 (2007) 3968–3976.
[16] K. Dejaeger, J. Criquet, M. Vanoppen, C. Vignal, G. Billon, E.R. Cornelissen, Identification of disinfection by-product precursors by natural organic matter fractionation: a review, Environ. Chem. Lett. 20 (2022) 3861–3882.
[17] Y. Liu, Q. Wang, S. Zhang, J. Lu, S. Yue, NOM reactivity with chlorine in low SUVA water, J. Water Supply Res. Technol. - Aqua 60 (2011) 231–239.
[18] I. Kristiana, J. Tan, C.A. Joll, A. Heitz, U. von Gunten, J.W.A. Charrois, Formation of N-nitrosamines from chlorination and chloramination of molecular weight fractions of natural organic matter, Water Res. 47 (2013) 535–546.
[19] J. Liu, E. Yang, T. Huang, Z. Wang, B. Dong, Correlation of chemically irreversible fouling with organic constituents of feed water during membrane filtration, Colloids Surf., A 597 (2020) 124790.
[20] Y. Liu, X. Li, Y. Yang, W. Ye, S. Ji, J. Ren, Z. Zhou, Analysis of the major particle-size based foulants responsible for ultrafiltration membrane fouling in polluted raw water, Desalination 347 (2014) 191–198.
[21] H. Yamamura, K. Okimoto, K. Kimura, Y. Watanabe, Hydrophilic fraction of natural organic matter causing irreversible fouling of microfiltration and ultrafiltration membranes, Water Res. 54 (2014) 123–136.
[22] N. Her, G. Amy, J. Chung, J. Yoon, Y. Yoon, Characterizing dissolved organic matter and evaluating associated nanofiltration membrane fouling, Chemosphere 70 (2008) 495–502.
[23] G. Hua, D.A. Reckhow, Characterization of disinfection byproduct precursors based on hydrophobicity and molecular size, Environ. Sci. Technol. 41 (2007) 3309–3315.
[24] M. Derrien, S.R. Brogi, R. Gonçalves-Araujo, Characterization of aquatic organic matter: assessment, perspectives and research priorities, Water Res. 163 (2019) 114908.

[25] S. Derenne, T.T. Nguyen Tu, Characterizing the molecular structure of organic matter from natural environments: an analytical challenge, C. R. Geosci. 346 (2014) 53–63.
[26] Y. Pan, H. Li, X. Zhang, A. Li, Characterization of natural organic matter in drinking water: sample preparation and analytical approaches, Trends Environ. Anal. Chem. 12 (2016) 23–30.
[27] J. Liu, Z. Wang, B. Dong, D. Zhao, Fouling behaviors correlating to water characteristics during the ultrafiltration of micro-polluted water with and without the addition of powdered activated carbon, Colloids Surf., A 511 (2016) 320–328.
[28] L. Fan, J.L. Harris, F.A. Roddick, N.A. Booker, Influence of the characteristics of natural organic matter on the fouling of microfiltration membranes, Water Res. 35 (2001) 4455–4463.
[29] Y. Bessiere, B. Jefferson, E. Goslan, P. Bacchin, Effect of hydrophilic/hydrophobic fractions of natural organic matter on irreversible fouling of membranes, Desalination 249 (2009) 182–187.
[30] W. Yin, X. Li, S.R. Suwarno, E.R. Cornelissen, T.H. Chong, Fouling behavior of isolated dissolved organic fractions from seawater in reverse osmosis (RO) desalination process, Water Res. 159 (2019) 385–396.
[31] A.W. Zularisam, A.F. Ismail, M.R. Salim, M. Sakinah, H. Ozaki, The effects of natural organic matter (NOM) fractions on fouling characteristics and flux recovery of ultrafiltration membranes, Desalination 212 (2007) 191–208.
[32] H.-K. Shon, S.-H. Kim, L. Erdei, S. Vigneswaran, Analytical methods of size distribution for organic matter in water and wastewater, Korean J. Chem. Eng. 23 (2006) 581–591.
[33] J. Engelke, J. Brandt, C. Barner-Kowollik, A. Lederer, Strengths and limitations of size exclusion chromatography for investigating single chain folding – current status and future perspectives, Polym. Chem. 10 (2019) 3410–3425.
[34] S. Podzimek, Asymmetric flow field flow fractionation, in: Light Scattering, Size Exclusion Chromatography and Asymmetric Flow Field Flow Fractionation, John Wiley & Sons, Hoboken, New Jersey, 2011, pp. 259–305.
[35] S.K.R. Williams, J.R. Runyon, A.A. Ashames, Field-flow fractionation: addressing the nano challenge, Anal. Chem. 83 (2011) 634–642.
[36] Y. Wang, C.W. Cuss, W. Shotyk, Application of asymmetric flow field-flow fractionation to the study of aquatic systems: coupled methods, challenges, and future needs, J. Chromatogr. A 1632 (2020) 461600.
[37] E. Zanardi-Lamardo, C.D. Clark, C.A. Moore, R.G. Zika, Comparison of the molecular mass and optical properties of colored dissolved organic material in two rivers and coastal waters by flow field-flow fractionation, Environ. Sci. Technol. 36 (2002) 2806–2814.
[38] C. Pelekani, G. Newcombe, V.L. Snoeyink, C. Hepplewhite, S. Assemi, R. Beckett, Characterization of natural organic matter using high performance size exclusion chromatography, Environ. Sci. Technol. 33 (1999) 2807–2813.
[39] J.R. Runyon, M. Ulmius, L. Nilsson, A perspective on the characterization of colloids and macromolecules using asymmetrical flow field-flow fractionation, Colloids Surf., A 442 (2014) 25–33.
[40] R. Manning, R. Holcomb, G. Wilson, C. Henry, M. Manning, Review of orthogonal methods to SEC for quantitation and characterization of protein aggregates, Biopharm Int. 27 (2014) 32.
[41] C.R.M. Bria, F. Afshinnia, P.W. Skelly, T.M. Rajendiran, P. Kayampilly, T. P. Thomas, V.P. Andreev, S. Pennathur, S. Kim Ratanathanawongs Williams, Asymmetrical flow field-flow fractionation for improved characterization of human plasma lipoproteins, Anal. Bioanal. Chem. 411 (2019) 777–786.
[42] M. Baalousha, B. Stolpe, J.R. Lead, Flow field-flow fractionation for the analysis and characterization of natural colloids and manufactured nanoparticles in environmental systems: a critical review, J. Chromatogr. A 1218 (2011) 4078–4103.
[43] K.G. Wahlund, J.C. Giddings, Properties of an asymmetrical flow field-flow fractionation channel having one permeable wall, Anal. Chem. 59 (1987) 1332–1339.
[44] C.L. Plavchak, W.C. Smith, C.R.M. Bria, S.K.R. Williams, New advances and applications in field-flow fractionation, Annu. Rev. Anal. Chem. 14 (2021) 257–279.
[45] M.M. Clark, Transport Modeling for Environmental Engineers and Scientists, second, Wiley, New Jersey, 2011.
[46] K.-J. Hwang, Y.-L. Hsu, K.-L. Tung, Effect of particle size on the performance of cross-flow microfiltration, Adv. Powder Technol. 17 (2006) 189–206.
[47] A. Gopalakrishnan, M. Bouby, A.I. Schäfer, Membrane-organic solute interactions in asymmetric flow field flow fractionation: interplay of hydrodynamic and electrostatic forces, Sci. Total Environ. 855 (2023) 158891.
[48] J.C. Giddings, The conceptual basis of field-flow fractionation, J. Chem. Educ. 50 (1973) 667.
[49] J.C. Giddings, Field-flow fractionation: analysis of macromolecular, colloidal, and particulate materials, Science 260 (1993) 1456–1465.
[50] E. Bolea, M.P. Gorriz, M. Bouby, F. Laborda, J.R. Castillo, H. Geckeis, Multielement characterization of metal-humic substances complexation by size exclusion chromatography, asymmetrical flow field-flow fractionation, ultrafiltration and inductively coupled plasma-mass spectrometry detection: a comparative approach, J. Chromatogr. A 1129 (2006) 236–246.
[51] M.E. Schimpf, M.P. Petteys, Characterization of humic materials by flow field-flow fractionation, Colloids Surf., A 120 (1997) 87–100.
[52] C.W. Cuss, I. Grant-Weaver, W. Shotyk, AF4-ICPMS with the 300 Da membrane to resolve metal-bearing “colloids” < 1 kDa: optimization, fractogram deconvolution, and advanced quality control, Anal. Chem. 89 (2017) 8027–8035.
[53] R. Beckett, Z. Jue, J.C. Giddings, Determination of molecular weight distributions of fulvic and humic acids using flow field-flow fractionation, Environ. Sci. Technol. 21 (1987) 289–295.
[54] Z. Zhou, L. Guo, A critical evaluation of an asymmetrical flow field-flow fractionation system for colloidal size characterization of natural organic matter, J. Chromatogr. A 1399 (2015) 53–64.
[55] E. Neubauer, S.J. Köhler, F. von der Kammer, H. Laudon, T. Hofmann, Effect of pH and stream order on iron and arsenic speciation in boreal catchments, Environ. Sci. Technol. 47 (2013) 7120–7128.
[56] G. Dublet, I. Worms, M. Frutschi, A. Brown, G.C. Zünd, B. Bartova, V. I. Slaveykova, R. Bernier-Latmani, Colloidal size and redox state of uranium species in the porewater of a pristine mountain wetland, Environ. Sci. Technol. 53 (2019) 9361–9369.
[57] I.A.M. Worms, H.E. Chmiel, J. Traber, N. Tofield-Pasche, V.I. Slaveykova, Dissolved organic matter and associated trace metal dynamics from river to lake, under ice-covered and ice-free conditions, Environ. Sci. Technol. 53 (2019) 14134–14143.
[58] X. Li, Z. Cao, Y. Du, Y. Zhang, J. Wang, X. Ma, P. Hu, Y. Luo, L. Wu, Multi-metal contaminant mobilizations by natural colloids and nanoparticles in paddy soils during reduction and reoxidation, J. Hazard Mater. 461 (2024) 132684.
[59] Y. Wang, C.W. Cuss, L. Pei, W. Shotyk, Resolving uncertainties in the quantification of trace elements within organic-rich boreal rivers for AF4-UV-ICP-MS analysis, Anal. Chem. 96 (2024) 6889–6897.
[60] Y.-H. Cai, A. Gopalakrishnan, Q. Dong, A.I. Schäfer, Removal of strontium by nanofiltration: role of complexation and speciation of strontium with organic matter, Water Res. 253 (2024) 121241.
[61] Y.-A. Boussouga, T. Okkali, T. Luxbacher, A.I. Schäfer, Chromium (III) and chromium (VI) removal and organic matter interaction with nanofiltration, Sci. Total Environ. 885 (2023) 163695.
[62] R.W. Baker, Reverse osmosis, in: Membrane Technology and Applications, John Wiley & Sons Ltd., 2004, pp. 191–235.
[63] P. Arribas, M. Khayet, M.C. García-Payo, L. Gil, 8 - novel and emerging membranes for water treatment by hydrostatic pressure and vapor pressure gradient membrane processes, in: A. Basile, A. Cassano, N.K. Rastogi (Eds.), Advances in Membrane Technologies for Water Treatment, Woodhead Publishing, Oxford, 2015, pp. 239–285.
[64] Lenntech, Molecular weight cutoff (MWCO). https://www.lenntech.com/services/mwco.htm. (Accessed 22 March 2023).
[65] I. Koyuncu, R. Sengur, T. Turken, S. Guclu, M.E. Pasaoglu, 3 - advances in water treatment by microfiltration, ultrafiltration, and nanofiltration, in: A. Basile, A. Cassano, N.K. Rastogi (Eds.), Advances in Membrane Technologies for Water Treatment, Woodhead Publishing, Oxford, 2015, pp. 83–128.
[66] M. Park, S.A. Snyder, Chapter 6 - attenuation of contaminants of emerging concerns by nanofiltration membrane: rejection mechanism and application in water reuse, in: A.J. Hernández-Maldonado, L. Blaney (Eds.), Contaminants of Emerging Concern in Water and Wastewater, Butterworth-Heinemann, 2020, pp. 177–206.
[67] A. Imbrogno, J.I. Calvo, M. Breida, R. Schwaiger, A.I. Schäfer, Molecular weight cut off (MWCO) determination in ultra- and nanofiltration: review of methods and implications on organic matter removal, Sep. Purif. Technol. 354 (2024) 128612.
[68] S. Guo, Y. Wan, X. Chen, J. Luo, Loose nanofiltration membrane custom-tailored for resource recovery, Chem. Eng. J. 409 (2021) 127376.
[69] P.J.M. Dycus, K.D. Healy, G.K. Stearman, M.J.M. Wells, Diffusion coefficients and molecular weight distributions of humic and fulvic acids determined by flow field-flow fractionation, Sep. Sci. Technol. 30 (1995) 1435–1453.
[70] N. Manh Thang, H. Geckeis, J.I. Kim, H.P. Beck, Application of the flow field flow fractionation (FFFF) to the characterization of aquatic humic colloids: evaluation and optimization of the method, Colloids Surf., A 181 (2001) 289–301.
[71] A. Siripinyanond, R.M. Barnes, D. Amarasiriwardena, Flow field-flow fractionation-inductively coupled plasma mass spectrometry for sediment bound trace metal characterization, J. Anal. At. Spectrom. 17 (2002) 1055–1064.
[72] M.J.M. Wells, Conductivity-dependent flow field-flow fractionation of fulvic and humic acid aggregates, Chromatography 2 (2015) 580–593.
[73] D. Amarasiriwardena, A. Siripinyanond, R.M. Barnes, Trace elemental distribution in soil and compost-derived humic acid molecular fractions and colloidal organic matter in municipal wastewater by flow field-flow fractionation-inductively coupled plasma mass spectrometry (flow FFF-ICP-MS), J. Anal. At. Spectrom. 16 (2001) 978–986.
[74] M.H. Moon, D.Y. Shin, N. Lee, E. Hwang, I.-H. Cho, Flow field-flow fractionation/multiangle light scattering of sodium hyaluronate from various degradation processes, J. Chromatogr. B 864 (2008) 15–21.
[75] S. Phuntsho, H.K. Shon, S. Vigneswaran, J. Cho, Assessing membrane fouling potential of humic acid using flow field-flow fractionation, J. Membr. Sci. 373 (2011) 64–73.
[76] Y. Ham, Y. Kim, Y. Ju, S. Lee, S. Hong, Characterization of natural organic matters using flow field-flow fractionation and its implication to membrane fouling, Desalin. Water Treat. 51 (2013) 6378–6391.
[77] U.B. Kavurt, M. Marioli, W.T. Kok, D. Stamatialis, Membranes for separation of biomacromolecules and bioparticles via flow field-flow fractionation, J. Chem. Technol. Biotechnol. 90 (2015) 11–18.
[78] N. Bendixen, S. Losert, C. Adlhart, M. Lattuada, A. Ulrich, Membrane–particle interactions in an asymmetric flow field flow fractionation channel studied with titanium dioxide nanoparticles, J. Chromatogr. A 1334 (2014) 92–100.
[79] D.H. Kim, J. Moon, J. Cho, Identification of natural organic matter (NOM) transport behavior near the membrane surface using flow field-flow-fractionation (fl-FFF) micro channel, J. Water Supply Res. Technol. - Aqua 54 (2005) 249–259.

[80] G. Yohannes, S.K. Wiedmer, M. Jussila, M.L. Riekkola, Fractionation of humic substances by asymmetrical flow field-flow fractionation, Chromatographia 61 (2005) 359–364.
[81] J. Moon, S. Lee, J.-H. Song, J. Cho, Membrane fouling indicator of effluent organic matter with nanofiltration for wastewater reclamation, as obtained from flow field-flow fractionation, Sep. Purif. Technol. 73 (2010) 164–172.
[82] M. Baalousha, J.R. Lead, Size fractionation and characterization of natural aquatic colloids and nanoparticles, Sci. Total Environ. 386 (2007) 93–102.
[83] A.D. Revchuk, I.H. Suffet, Ultrafiltration separation of aquatic natural organic matter: chemical probes for quality assurance, Water Res. 43 (2009) 3685–3692.
[84] I. Mijatović, M. Matošić, B. Hajduk Černeha, D. Bratulić, Removal of natural organic matter by ultrafiltration and nanofiltration for drinking water production, Desalination 169 (2004) 223–230.
[85] A.I. Schäfer, A. Pihlajamäki, A.G. Fane, T.D. Waite, M. Nyström, Natural organic matter removal by nanofiltration: effects of solution chemistry on retention of low molar mass acids versus bulk organic matter, J. Membr. Sci. 242 (2004) 73–85.
[86] A.I. Schäfer, R. Mauch, T.D. Waite, A.G. Fane, Charge effects in the fractionation of natural organics using ultrafiltration, Environ. Sci. Technol. 36 (2002) 2572–2580.
[87] A.I. Schäfer, Natural Organics Removal Using Membranes: Principles, Performance, and Cost, First, CRC Press, Florida, 2001.
[88] E. Dulekgurgen, S. Doğruel, Ö. Karahan, D. Orhon, Size distribution of wastewater COD fractions as an index for biodegradability, Water Res. 40 (2006) 273–282.
[89] B.H. Gursoy-Haksevenler, I. Arslan-Alaton, Effects of treatment on the characterization of organic matter in wastewater: a review on size distribution and structural fractionation, Water Sci. Technol. 82 (2020) 799–828.
[90] E. Worch, Eine neue Gleichung zur Berechnung von Diffusionskoeffizienten gelöster Stoffe, Vom Wasser 81 (1993) 289–297.
[91] B. Van der Bruggen, J. Schaep, D. Wilms, C. Vandecasteele, Influence of molecular size, polarity and charge on the retention of organic molecules by nanofiltration, J. Membr. Sci. 156 (1999) 29–41.
[92] Y.-H. Cai, A. Gopalakrishnan, K.P. Deshmukh, A.I. Schäfer, Renewable energy powered membrane technology: implications of adhesive interaction between membrane and organic matter on spontaneous osmotic backwash cleaning, Water Res. (2022) 118752.
[93] Y. Ham, Y. Kim, Y. Ju, S. Lee, S. Hong, Characterization of natural organic matters using flow field-flow fractionation and its implication to membrane fouling, Desalin. Water Treat. 51 (2013) 6378–6391.
[94] E. Bolea, J. Jiménez-Lamana, F. Laborda, J. Castillo, Size characterization and quantification of silver nanoparticles by asymmetric flow field-flow fractionation coupled with inductively coupled plasma mass spectrometry, Anal. Bioanal. Chem. 401 (2011) 2723–2732.
[95] A. Ulrich, S. Losert, N. Bendixen, A. Al-Kattan, H. Hagendorfer, B. Nowack, C. Adlhart, J. Ebert, M. Lattuada, K. Hungerbühler, Critical aspects of sample handling for direct nanoparticle analysis and analytical challenges using asymmetric field flow fractionation in a multi-detector approach, J. Anal. At. Spectrom. 27 (2012) 1120–1130.
[96] S. Podzimek, C. Johann, Asymmetric flow field-flow fractionation: current status, possibilities, analytical limitations and future trends, Chromatographia (2021) 531–534.
[97] M.R. Teixeira, V.S. Sousa, Fouling of nanofiltration membrane: effects of NOM molecular weight and microcystins, Desalination 315 (2013) 149–155.
[98] A.S. Al-Amoudi, Factors affecting natural organic matter (NOM) and scaling fouling in NF membranes: a review, Desalination 259 (2010) 1–10.
[99] F.A. Messaud, R.D. Sanderson, J.R. Runyon, T. Otte, H. Pasch, S.K.R. Williams, An overview on field-flow fractionation techniques and their applications in the separation and characterization of polymers, Prog. Polym. Sci. 34 (2009) 351–368.
[100] Postnova Analytics GmbH, NovaFFF AF2000 Software Manual, Landsberg, Germany, 2017, pp. 1–144, Version 2.0.9.9.
[101] Postnova Analytics GmbH, AF2000 MF Operation Manual, Landsberg, Germany, 2016, pp. 1–60.
[102] A. Imbrogno, A.I. Schäfer, Comparative study of nanofiltration membrane characterization devices of different dimension and configuration (cross flow and dead end), J. Membr. Sci. 585 (2019) 67–80.
[103] Y.-A. Boussouga, F. Tantish, A.I. Schäfer, Microporous hematite-loaded composite membrane for arsenic(III) and arsenic(V) removal, ACS Appl. Eng. Mater. 1 (2023) 1164–1175.
[104] A. Imbrogno, J. Biscarat, A.I. Schafer, Estradiol uptake in a combined magnetic ion exchange - ultrafiltration (MIEX-UF) process during water treatment, Curr. Pharm. Des. 23 (2017) 328–337.
[105] K. Boussu, Y. Zhang, J. Cocquyt, P. Van der Meeren, A. Volodin, C. Van Haesendonck, J.A. Martens, B. Van der Bruggen, Characterization of polymeric nanofiltration membranes for systematic analysis of membrane performance, J. Membr. Sci. 278 (2006) 418–427.
[106] Y.-A. Boussouga, H. Frey, A.I. Schäfer, Removal of arsenic(V) by nanofiltration: impact of water salinity, pH and organic matter, J. Membr. Sci. 618 (2021) 118631.
[107] Postnova Analytics GmbH, AF2000 MF Supplies and Consumables Brochure, Landsberg, Germany, 2021.
[108] Nitto Hydranautics, HYDRACoRe10 and 50 LD 4040 Series, California, USA.
[109] Y.-A. Boussouga, M.B. Mohankumar, A. Gopalakrishnan, A. Welle, A.I. Schäfer, Removal of arsenic(III) via nanofiltration: contribution of organic matter interactions, Water Res. 201 (2021) 117315.
[110] Y.-H. Cai, A.I. Schäfer, Renewable energy powered membrane technology: impact of solar irradiance fluctuation on direct osmotic backwash, J. Membr. Sci. 598 (2020) 117666.
[111] L.G. Sharma, L.M. Pandey, Thermomechanical process induces unfolding and fibrillation of bovine serum albumin, Food Hydrocolloids 112 (2021) 106294.
[112] Y.-A. Boussouga, F. Sacher, A.I. Schäfer, Water quality of the Gambia River: a prospective drinking water supply, Sci. Total Environ. 878 (2023) 162794.
[113] J. Shen, A.I. Schäfer, Factors affecting fluoride and natural organic matter (NOM) removal from natural waters in Tanzania by nanofiltration/reverse osmosis, Sci. Total Environ. 527–528 (2015) 520–529.
[114] G. Abbt-Braun, F.H. Frimmel, P. Lipp, Isolation of organic substances from aquatic and terrestrial systems-comparison of some methods, Z. Wasser-Abwasser-Forsch. 24 (1991) 285–292.
[115] S. Valencia, J.M. Marín, G. Restrepo, F.H. Frimmel, Evaluation of natural organic matter changes from Lake Hohloh by three-dimensional excitation–emission matrix fluorescence spectroscopy during TiO2/UV process, Water Res. 51 (2014) 124–133.
[116] E. Neubauer, F.v.d. Kammer, T. Hofmann, Influence of carrier solution ionic strength and injected sample load on retention and recovery of natural nanoparticles using flow field-flow fractionation, J. Chromatogr. A 1218 (2011) 6763–6773.
[117] S.A. Huber, A. Balz, M. Abert, W. Pronk, Characterisation of aquatic humic and non-humic matter with size-exclusion chromatography – organic carbon detection – organic nitrogen detection (LC-OCD-OND), Water Res. 45 (2011) 879–885.
[118] M. Klučáková, Size and charge evaluation of standard humic and fulvic acids as crucial factors to determine their environmental behavior and impact, Front. Chem. 6 (2018).
[119] F. Loosli, L. Vitorazi, J.-F. Berret, S. Stoll, Towards a better understanding on agglomeration mechanisms and thermodynamic properties of TiO2 nanoparticles interacting with natural organic matter, Water Res. 80 (2015) 139–148.
[120] A. Imbrogno, M.N. Nguyen, A.I. Schäfer, Tutorial review of error evaluation in experimental water research at the example of membrane filtration, Chemosphere 357 (2024) 141833.
[121] B. Meisterjahn, S. Wagner, F. von der Kammer, D. Hennecke, T. Hofmann, Silver and gold nanoparticle separation using asymmetrical flow-field flow fractionation: influence of run conditions and of particle and membrane charges, J. Chromatogr. A 1440 (2016) 150–159.
[122] M.N. Nguyen, R. Hérvas-Martínez, A.I. Schäfer, Organic matter interference with steroid hormone removal by single-walled carbon nanotubes – ultrafiltration composite membrane, Water Res. 199 (2021) 117148.
[123] S. Schachermeyer, J. Ashby, M. Kwon, W. Zhong, Impact of carrier fluid composition on recovery of nanoparticles and proteins in flow field flow fractionation, J. Chromatogr. A 1264 (2012) 72–79.
[124] M. Marioli, W.T. Kok, Recovery, overloading, and protein interactions in asymmetrical flow field-flow fractionation, Anal. Bioanal. Chem. 411 (2019) 2327–2338.
[125] T. Kowalkowski, M. Sugajski, B. Buszewski, Impact of ionic strength of carrier liquid on recovery in flow field-flow fractionation, Chromatographia 81 (2018) 1213–1218.
[126] J. Gigault, J.M. Pettibone, C. Schmitt, V.A. Hackley, Rational strategy for characterization of nanoscale particles by asymmetric-flow field flow fractionation: a tutorial, Anal. Chim. Acta 809 (2014) 9–24.
[127] H. Dou, E.C. Jung, S. Lee, Factors affecting measurement of channel thickness in asymmetrical flow field-flow fractionation, J. Chromatogr. A 1393 (2015) 115–121.
[128] M. Elimelech, J. Gregory, X. Jia, R.A. Williams, Chapter 3 - surface interaction potentials, in: M. Elimelech, J. Gregory, X. Jia, R.A. Williams (Eds.), Particle Deposition & Aggregation, Butterworth-Heinemann, Woburn, 1995, pp. 33–67.
[129] A.K. Zander, N.K. Curry, Membrane and solution effects on solute rejection and productivity, Water Res. 35 (2001) 4426–4434.
[130] M.A. Benincasa, J.C. Giddings, Separation and characterization of cationic, anionic, and nonionic water-soluble polymers by flow FFF: sample recovery, overloading, and ionic strength effects, J. Microcolumn Sep. 9 (1997) 479–495.
[131] R. Suwanpetch, J. Shiowatana, A. Siripinyanond, Using flow field-flow fractionation (Fl-FFF) for observation of salinity effect on the size distribution of humic acid aggregates, Int. J. Environ. Anal. Chem. 97 (2017) 217–229.
[132] M.-A. Benincasa, G. Cartoni, N. Imperia, Effects of ionic strength and electrolyte composition on the aggregation of fractionated humic substances studied by flow field-flow fractionation, J. Sep. Sci. 25 (2002) 405–415.
[133] S. Hong, M. Elimelech, Chemical and physical aspects of natural organic matter (NOM) fouling of nanofiltration membranes, J. Membr. Sci. 132 (1997) 159–181.
[134] H. Zhang, H. Wang, J. Wang, R. Guo, Q. Zhang, The effect of ionic strength on the viscosity of sodium alginate solution, Polym. Adv. Technol. 12 (2001) 740–745.
[135] X. Fu, J. Pan, H. Xu, Characterization and modification of the molecular weight distribution within dissolved organic matter using flow field-flow fractionation, Limnol Oceanogr. Methods 18 (2020) 560–569.